The Plant Cell, Vol. 25: 851–867, March 2013, www.plantcell.org

MAP18 Regulates the Direction of Pollen Tube Growth in *Arabidopsis* by Modulating F-Actin Organization[C][W][OA]

Lei Zhu,[1] Yan Zhang,[1] Erfang Kang, Qiangyi Xu, Miaoying Wang, Yue Rui, Baoquan Liu, Ming Yuan, and Ying Fu[2]

State Key Laboratory of Plant Physiology and Biochemistry, College of Biological Sciences, China Agricultural University, Beijing 100193, China

For fertilization to occur in plants, the pollen tube must be guided to enter the ovule via the micropyle. Previous reports have implicated actin filaments, actin binding proteins, and the tip-focused calcium gradient as key contributors to polar growth of pollen tubes; however, the regulation of directional pollen tube growth is largely unknown. We reported previously that *Arabidopsis thaliana* MICROTUBULE-ASSOCIATED PROTEIN18 (MAP18) contributes to directional cell growth and cortical microtubule organization. The preferential expression of *MAP18* in pollen and in pollen tubes suggests that MAP18 also may function in pollen tube growth. In this study, we demonstrate that MAP18 functions in pollen tubes by influencing actin organization, rather than microtubule assembly. In vitro biochemical results indicate that MAP18 exhibits Ca^{2+}-dependent filamentous (F)-actin-severing activity. Abnormal expression of *MAP18* in *map18* and *MAP18 OX* plants was associated with disorganization of the actin cytoskeleton in the tube apex, resulting in aberrant pollen tube growth patterns and morphologies, inaccurate micropyle targeting, and fewer fertilization events. Experiments with MAP18 mutants created by site-directed mutagenesis suggest that F-actin-severing activity is essential to the effects of MAP18 on pollen tube growth direction. Our study demonstrates that in *Arabidopsis*, MAP18 guides the direction of pollen tube growth by modulating actin filaments.

INTRODUCTION

Pollen tube growth is a rapid and polarized process that occurs exclusively at the tube tip and involves the elongation of pollen tubes within the female reproductive tissues to deliver sperm cells to ovules for fertilization. The actin cytoskeleton plays critical roles in pollen tube growth (Gibbon et al., 1999; Fu et al., 2001; Hepler et al., 2001; Vidali and Hepler, 2001; Vidali et al., 2001) by supporting organelle movements and cytoplasmic streaming and by regulating vesicle trafficking in the tip zone (Cárdenas et al., 2005; Cheung and Wu, 2008; Dhonukshe et al., 2008; Cheung et al., 2010; Staiger et al., 2010). The pollen tube is comprised of the shank, the subapex, and the apex, which each exhibit distinctly organized filamentous (F)-actin (Geitmann and Emons, 2000; Vidali and Hepler, 2001). These actin structures may perform diverse functions. Organelles and secretory vesicles are trafficked along longitudinal actin cables throughout the shank of elongating pollen tubes (Hepler et al., 2001; Cheung et al., 2002). In the subapical region, actin molecules are highly dynamic and form a dense mesh of short, randomly oriented filaments (Geitmann and Emons, 2000; Vidali et al., 2001; Chen et al., 2002). Rapid actin remodeling in the subapex may reverse cytoplasmic flows and support pollen tube elongation (Hepler et al., 2001). Long actin filaments in the shank extend into the subapical region but do not reach the apical region, where only short and fine F-actin are observed (Kost et al., 1999; Fu et al., 2001). Apical actin filaments likely regulate exocytic vesicle docking and fusion (Lee et al., 2008; Kroeger et al., 2009; Bou Daher and Geitmann, 2011).

The intracellular Ca^{2+} concentration is elevated at the extreme tip of pollen tubes, creating a gradient that is necessary for pollen tube elongation (Pierson et al., 1994; Schiøtt et al., 2004; Iwano et al., 2009). In vivo studies have reported that the apical actin cytoskeleton is remodeled during pollen tube elongation and the dynamics of apical F-actin correlate with the oscillation of the Ca^{2+} gradient at the tip (Kost et al., 1999; Fu et al., 2001; Gu et al., 2005; Hwang et al., 2005).

During pollen tube extension, the growth direction is continuously reoriented by external signals and physical obstacles (Cheung and Wu, 2001). This guided growth is regulated by signaling pathways involving membrane receptor kinases and the Ras-homologous (Rho) family of small guanine nucleotide-binding proteins (GTPases). In addition, variations in ion fluxes may regulate actin organization as a downstream effect in the reorientation response (Camacho and Malhó, 2003; Chen et al., 2003; Kaothien et al., 2005; Bou Daher and Geitmann, 2011). Alternatively, an adjustment in the Ca^{2+} gradient in the tip region reorients growth direction (Pierson et al., 1994; Holdaway-Clarke et al., 2003). F-actin and the oscillation of the Ca^{2+} gradient in the apex modulate the accumulation of secretory vesicles and their fusion with specific regions of the apical plasma membrane (Kost et al., 1999; Fu et al., 2001; Gu et al., 2005; Hwang et al., 2005; Lee et al., 2008; McKenna et al., 2009; Cheung et al., 2010).

[1] These authors contributed equally to this work.
[2] Address correspondence to yingfu@cau.edu.cn.
The author responsible for distribution of materials integral to the findings presented in this article in accordance with the policy described in the Instructions for Authors (www.plantcell.org) is: Ying Fu (yingfu@cau.edu.cn).
[C] Some figures in this article are displayed in color online but in black and white in the print edition.
[W] Online version contains Web-only data.
[OA] Open Access articles can be viewed online without a subscription.
www.plantcell.org/cgi/doi/10.1105/tpc.113.110528

The organization and dynamics of F-actin and the equilibrium between globular (G)-actin and F-actin pools are regulated by several classes of actin binding proteins (ABPs; Staiger, 2000; Hussey et al., 2006; Ren and Xiang, 2007; Chen et al., 2009; Fu, 2010) that respond to environmental cues and cellular signals, including Ca^{2+}, pH, phosphorylation, and phosphoinositides (Franklin-Tong, 1999; Hepler et al., 2001; Monteiro et al., 2005; Ren and Xiang, 2007). Formins, villins, and actin-depolymerizing factors (ADFs) are important for maintaining the organization of the actin cytoskeleton to support pollen tube growth (Chen et al., 2003; Cheung and Wu, 2004). *Arabidopsis thaliana* formin homology5 (FH5), a tip-localized and cell membrane–anchored protein, nucleates the subapical actin assembly and the apical vesicular organization and is critical for tip-focused growth of pollen tubes (Cheung et al., 2010). Of the identified villin family proteins, most function to sever or bundle F-actin in a Ca^{2+}-dependent manner (Yokota et al., 2000, 2003, 2005; Yokota and Shimmen, 1998). In *Arabidopsis*, VILLIN3 (VLN3) severs actin filaments, is regulated by Ca^{2+}, and contributes to bundle turnover (Khurana et al., 2010). VLN5 is a major F-actin-stabilizing factor that regulates actin dynamics in concert with oscillatory Ca^{2+} gradients to facilitate pollen tube growth (Zhang et al., 2010). ACTIN BINDING PROTEIN29 (ABP29) is a splice variant of *Lilium longiflorum* Villin and a member of the villin/gelsolin/fragmin superfamily that accelerates actin nucleation, blocks barbed ends, and severs actin filaments in Ca^{2+} and/or phosphatidylinositol 4,5-bisphosphate–dependent manners in vitro (Xiang et al., 2007). In addition, ABP29 contributes to actin cytoskeletal rearrangements during pollen germination and tube growth (Xiang et al., 2007).

MICROTUBULE-ASSOCIATED PROTEIN18 (MAP18) regulates cortical microtubule organization by destabilizing associated microtubules, thereby modulating polar cell growth in vegetative tissues (Wang et al., 2007). Our previous β-glucuronidase (GUS) activity analysis, a search of the Genevestigator database (https://www.genevestigator.com/gv/), and data from the *Arabidopsis* pollen GeneChip (Wang et al., 2007; Wang et al., 2008) indicated that *MAP18* is expressed primarily in pollen. Similarly, Kato et al. (2010) reported that the *plasma membrane–associated Ca^{2+} binding protein2* (*PCaP2*)/*MAP18* gene was expressed strongly in developing root hairs and elongating pollen tubes. These data implicate MAP18 in the regulation of pollen tube growth.

In this study, we characterize a novel function of MAP18: its control of pollen tube growth direction independent of elongation. We demonstrate that MAP18 exhibits Ca^{2+}-dependent F-actin-severing activity in vitro. Abnormal expression of *MAP18* affects F-actin organization in pollen tubes, which leads to swollen tips and bending growth patterns of in vitro–germinated pollen tubes as well as the reduction of micropyle targeting and fertilization events in vivo. Our results highlight MAP18 as a key modulator of pollen tube growth direction.

RESULTS

MAP18 Is Required for Normal Pollen Tube Growth in Vitro

We demonstrated previously that *MAP18* (At5g44610) was expressed in rapidly elongating regions of root and flower tissues (Wang et al., 2007). Data from the Affymetrix AG and ATH1 GeneChip arrays (https://www.genevestigator.com/gv/) suggest that *MAP18* is expressed primarily in male flower tissues. The *Arabidopsis* pollen GeneChip indicates that *MAP18* is elevated in growing pollen tubes compared with germinating or hydrated pollens (Wang et al., 2008). Kato et al. (2010) also reported strong expression of the *PCaP2* (*MAP18*) gene in elongating root hairs and pollen tubes. To verify these observations, transgenic lines transformed with a *MAP18* promoter-driven GUS reporter were generated. GUS activity then was measured from mature pollen grains and germinated pollen tubes in vitro (see Supplemental Figure 1A online).

To investigate the function of MAP18 in pollen tubes, we obtained the T-DNA insertion line *map18* from the ABRC (SALK_021652) (see Supplemental Figure 1B online). Quantitative RT-PCR (qRT-PCR) analysis indicated that *map18* is a knockdown mutant (see Supplemental Figure 1C online). Pollen grains from wild-type and *map18* plants were germinated in vitro on *Arabidopsis* pollen medium and were observed 4 h after germination. The germination rates of *map18* pollen grains were similar to those of wild-type pollen grains ($P > 0.1$, Student's *t* test) (Figures 1A and 1C). Moreover, no obvious differences were observed in the mean length of pollen tubes between *map18* and wild-type specimens ($P > 0.1$, Student's *t* test) (Figures 1A and 1C). However, *map18* pollen tubes displayed bending growth patterns with markedly swollen tip regions (Figure 1B). The mean width of pollen tubes was significantly increased in *map18* (12.9 ± 1.1 μm) compared with the wild type (7.4 ± 0.9 μm, $P < 0.01$, Student's *t* test) (Figure 1C). Measurements of the net angles of pollen tube growth showed that most wild-type pollen tubes grew at an average net angle of $10.1 \pm 1.1°$. By contrast, *map18* pollen tubes bended at a significantly larger average net angle of $29.3 \pm 2.4°$ ($P < 0.01$, Student's *t* test) (Figures 1B and 1C).

The abnormal growth phenotype of *map18* was rescued following transformation with a *MAP18promoter:MAP18-eGFP* (for enhanced green fluorescent protein) construct. Fifteen of 18 independently transformed lines recovered the swollen-tip phenotype in pollen tubes. Two of these lines (COM#1 and COM#9) were selected for further phenotypic analysis (Figure 1B; see Supplemental Figure 1C online). We concluded that the defects observed in *map18* pollen tubes resulted from downregulation of *MAP18* expression and that MAP18 is required for normal pollen tube growth. The complementation of the *map18* pollen tube phenotype by *MAP18-eGFP* indicated that MAP18-eGFP could functionally replace endogenous MAP18.

Abnormal Expression of *MAP18* Leads to Abnormal Pollen Tube Growth and a Fertilization Defect in Vivo

To understand the function of MAP18 in pollen tubes in vivo, *MAP18* overexpression lines were generated by expressing *MAP18pro:MAP18-eGFP* in the wild-type background (Columbia [Col]). The severity of the wavy-tube phenotype correlated with the expression levels of *MAP18* revealed by qRT-PCR analysis and with the fluorescence levels observed under the same microscope setting in the *MAP18-eGFP* pollen tubes (see Supplemental Figure 2 online), suggesting an association between expression levels of MAP18-eGFP and the induced pollen tube phenotype. Line #3 was chosen for further analyses and named *MAP18 OX*.

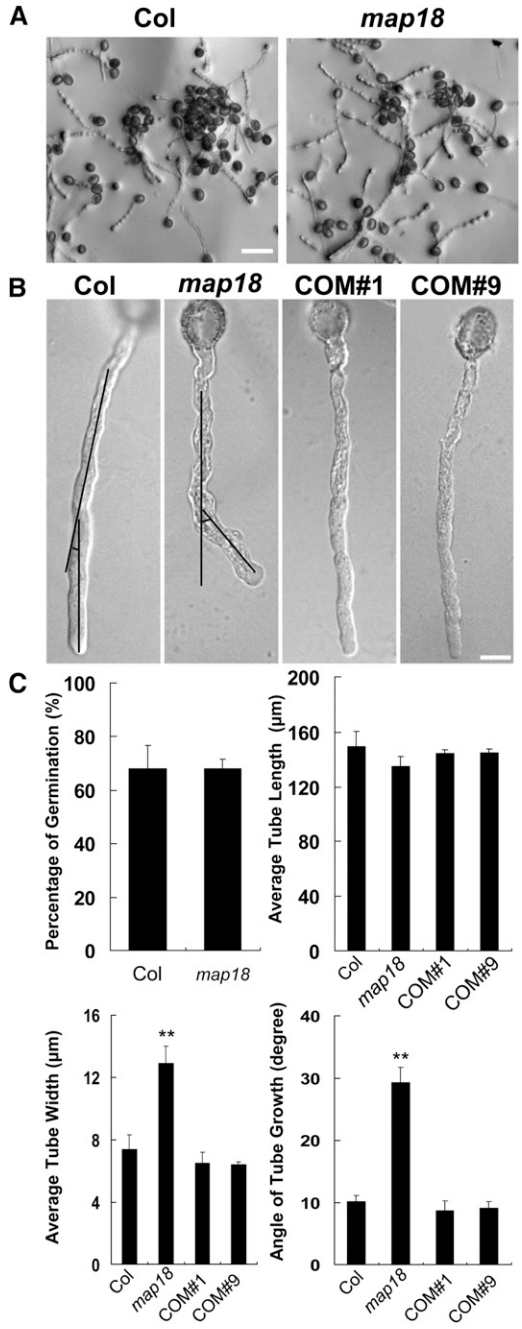

Figure 1. *MAP18* Is Required for Normal Pollen Tube Growth.

(A) Pollen grains from *Arabidopsis* wild-type Col and *map18* mutants were germinated in vitro. Images of pollen tubes were obtained at 4 h after germination. Bar = 100 μm.

(B) Representative images of pollen tubes from wild-type Col, *map18*, and complemented lines COM#1 and COM#9. Black lines indicate the angles between the initial directions and the turning directions of growing pollen tubes, which are measured in **(C)**. Bar = 10 μm.

(C) Germination percentage, length of pollen tubes, width of tube tips, and angles of growing tubes were measured (n > 120 pollen tubes). No substantial differences in the germination rates and pollen tube lengths were observed between wild-type and *map18* pollen tubes; however, the mean tube tip width and the mean angle of growing tubes were increased significantly in *map18* pollen tubes. Error bars represent ± SD based on three independent experiments. **P < 0.01, by Student's t test.

We next examined the pollen tube growth in the stigmata and styles of wild-type, *MAP18 OX*, and *map18* plants. Pollen tubes were fixed and stained with aniline blue at 2 h or 24 h after pollination and were observed using fluorescence microscopy. At 2 h after self-pollination, wild-type, *map18*, and *MAP18 OX* pollen had germinated and pollen tubes penetrated into stigmatic tissues to reach the top of the transmitting tracts (Figures 2A to 2C). No significant differences were detected in the maximum lengths or overall morphologies of wild-type, *map18*, and *MAP18 OX* pollen tubes. This was consistent with the observation that knocking down *MAP18* did not affect the germination or growth rates of pollen tubes in vitro.

A growth defect was revealed in *map18* and *MAP18 OX* plants at 24-h after self-pollination when most wild-type, *map18*, and *MAP18 OX* pollen tubes had reached the bottom of the transmitting tracts and had targeted ovules (Figures 2D to 2F). Wild-type pollen tubes grew along the funiculi and directly toward the ovules (Figure 2D). By contrast, *map18* pollen tubes exhibited aberrant growth, extensively elongating outward from the transmitting tract (Figure 2E, closed arrowhead) or exhibiting meandering patterns around the micropyles (Figure 2G). These defects were absent in *map18* pistils pollinated with wild-type pollen (Figure 2G), suggesting that MAP18 did not affect the female gametophyte. The growth of *MAP18 OX* pollen tubes also exhibited disordered and entangled patterns in the transmitting tract (Figure 2F). Although more than half of the pollen tubes could eventually target micropyles, we observed a wandering growth behavior along the pathway (Figure 2H), and some pollen tubes failed to reach ovules (Figure 2F, open arrowhead). These defects were not observed in *MAP18 OX* pistils pollinated with wild-type pollen (Figure 2H).

To quantify this phenotype, the relative distance ratio (i.e., the distance of the pollen tube growth path divided by the direct distance between the transmitting tract and micropyle) (Figure 2I, inset) was calculated. The relative distance ratio was 1.3 ± 0.3 in wild-type pollen tubes (n = 48), 2.1 ± 0.4 (n = 28) in *map18* pollen tubes, and 1.8 ± 0.5 (n = 28) in *MAP18 OX* pollen tubes (Figure 2I). These quantitative results confirmed the visual observations of abnormal pollen tube growth in *map18* and *MAP18 OX* plants. These results suggest that MAP18 plays an important role in regulating growth direction and targeting of pollen tubes.

Because a change in *MAP18* expression level caused a male-specific transmission defect, we expected to observe a concomitant defect in embryonic fertilization. Therefore, we examined wild-type and *map18* siliques. All *map18* siliques contained substantial seed gaps (Figure 2J, arrows) and unfertilized ovules (Figure 2K, asterisks). The proportion of overall seed setting was 82% (750 seeds total scored in 15 siliques from 10 *map18* plants). In *MAP18 OX* siliques, seeds were reduced even more dramatically, and the proportion of seed setting was 65% (Figure 2L). In comparison, wild-type siliques contained virtually no unfertilized ovules. This defect was rescued in COM#1. However, no aborted

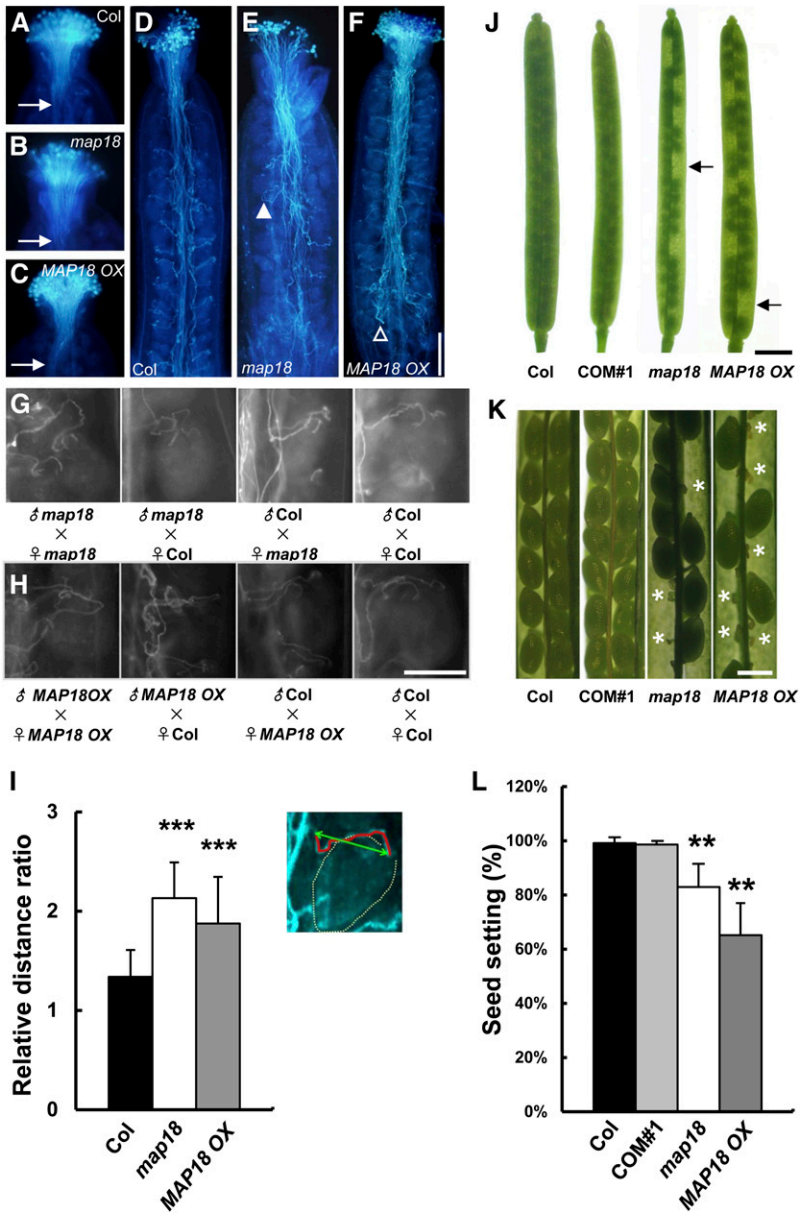

Figure 2. Altered Expression of MAP18 Interferes with Pollen Tube Growth and Fertilization of Embryos.

(A) to **(C)** Pollen grains from *Arabidopsis* wild-type Col **(A)**, *map18* mutants **(B)**, and *MAP18 OX* **(C)** were used to self-pollinate stigmata. Grains were then incubated for 2 h before fixation and staining with aniline blue. Pollen tubes from each line penetrated the stigmatic tissue similarly and reached the top of the transmitting tracts. Arrows indicate pollen tubes in transmitting tracts.

(D) to **(F)** Following 24 h incubation, wild-type Col **(D)**, *map18* mutants **(E)**, and *MAP18 OX* **(F)** pollen tubes all reached the bottom of the transmitting tracts and had grown toward ovules.

(D) Wild-type pollen tubes grew along the funiculus and directly toward the ovule.

(E) The *map18* pollen tubes elongated markedly outward from the transmitting tract (closed arrowhead).

(F) *MAP18 OX* pollen tubes exhibited disordered and entangled patterns in the transmitting tract with some pollen tubes failing to target to ovules (open arrowhead). Bar in **(F)** = 200 μm for **(A)** to **(F)**.

(G) Pollen grains from wild-type Col and *map18* were used to pollinate self or nonself stigmata. The self-pollinated *map18* pollen tubes exhibit meandering growth patterns around the micropyles, but no defect is observed when *map18* pistils are pollinated with wild-type pollen.

(H) Pollen grains from wild-type Col and *MAP18 OX* were used for self or nonself pollination. The self-pollinated *MAP18 OX* pollen tubes exhibit wandering growth characteristics around the micropyles. These defects are not observed when *MAP18 OX* pistils are pollinated with wild-type pollen. Bar in **(H)** = 100 μm for **(G)** and **(H)**.

ovules were observed when wild-type pollen was used to pollinate *map18* pistils. These data indicate that MAP18 regulates pollen tube growth direction and fertilization.

MAP18 Is Important for F-Actin Organization in the Apical and Subapical Regions

We previously identified MAP18 as a microtubule-associated protein (Wang et al., 2007). However, subsequent reports suggested that the microtubule cytoskeleton was not a major contributor to pollen tube tip growth (Cheung et al., 2008; Cai and Cresti, 2009). We investigated whether the pollen tube phenotype of *map18* mutants resulted from a change in microtubule organization by observing microtubules in pollen tubes using immunofluorescent microscopy. Microtubules were organized as bundles along the elongation axis in the shank region, and few microtubules were detected in the apical domain in *map18*. These findings were identical to our observations of wild-type pollen tubes (see Supplemental Figure 3A online). We measured the skewness of the fluorescence intensity distribution of microtubules to evaluate the extent of microtubule bundling in the shank region of pollen tubes (this analysis is now widely used to quantify the extent of bundling of F-actin; Higaki et al., 2010). As shown in Supplemental Figure 3B online, microtubule bundling in *map18* pollen tubes was similar to that in wild-type tubes. We then measured the percentage of occupancy of microtubules in pollen tubes, and no significant difference was detected between *map18* pollen tubes and wild-type tubes (see Supplemental Figure 3B online). Therefore, the loss of MAP18 did not significantly impact microtubule organization in pollen tubes.

Next, we observed F-actin organization in pollen tubes using *lifeact-mEGFP* driven by the pollen-specific promoter *Lat52* under a spinning disc confocal microscope. In wild-type pollen tubes, actin cables were aligned longitudinally in the shank (Figure 3A), and a few highly dynamic fine F-actin structures were observed in the pollen tube tips (Figure 3D; see Supplemental Movie 1 online). Although longitudinal actin cables in the shanks appeared relatively normal across wild-type, *map18*, and *MAP18 OX* pollen tubes (Figures 3A to 3C), obvious differences were observed in the apical regions (Figures 3D to 3F).

In ~81% of *map18* pollen tubes (n = 32), slightly bending longitudinal actin cables protruded into the apical regions (Figure 3B), rather than terminating at the base of the subapical regions of the pollen tubes. Moreover, fine F-actin structures were rarely observed in the apex (Figure 3E; see Supplemental Movie 2 online). Similar features were identified in ~6% of wild-type pollen tubes (n = 32) but not in any *MAP18 OX* pollen tubes observed (0%, n = 32). In *MAP18 OX* pollen tubes, thick longitudinal actin cables were observed in the shank regions (Figure 3C), and excessive fine F-actin structures were formed and scattered in the tip (Figure 3F; see Supplemental Movie 3 online).

To quantify the defects of F-actin organization caused by abnormal expression of MAP18, we first measured the skewness in growing pollen tubes. As shown in Figure 3G, more F-actin bundles existed in apical and subapical regions of *map18* pollen tubes than in wild-type or *MAP18 OX* tubes. The mean skewness value was significantly increased in *map18* pollen tubes (4.62 ± 0.39, n = 10) compared with that of the wild type (3.84 ± 0.35, n = 10; $P < 0.001$, Student's t test). By contrast, the mean skewness value in *MAP18 OX* tubes was decreased to 3.43 ± 0.38 (n = 10, $P < 0.05$, Student's t test). Next, we counted the number of short filament fragments (length <2 μm) in growing pollen tube tips. More short apical F-actin fragments were displayed in *MAP18 OX* pollen tubes than in wild-type pollen tubes, but they were hardly seen in *map18* pollen tubes (Figure 3H).

All these observations suggested that the knockdown or overexpression of *MAP18* can influence actin organization in the apical and subapical regions of growing pollen tubes.

MAP18 Binds and Severs F-Actin in a Ca^{2+}-Dependent Manner in Vitro

Considering that MAP18 might function as an ABP rather than a microtubule-associated protein in pollen tubes, we conducted a biochemical analysis of MAP18.

Recombinant GST-MAP18 protein was prepared and purified. The ability of MAP18 to bind F-actin was examined using high-speed cosedimentation assays. Preformed F-actin (polymerized from 2 μM G-actin) was incubated with various concentrations of recombinant GST-MAP18. Following centrifugation, supernatants and pellets were harvested and analyzed using SDS-PAGE. GST-MAP18 cosedimented with F-actin in a dose-dependent manner and reached saturation in the presence of 7 μM GST-MAP18 (Figures 4A and 4B). The molar binding ratio of the recombinant protein to actin was estimated as ~0.6:1 at the saturation level (Figure 4B). To determine the equilibrium dissociation constant (K_d) value for this interaction, MAP18 in the pellet ($[MAP18]_{bound}$) was plotted as a function of MAP18 in the

Figure 2. (continued).

(I) Inset indicates a diagram for calculation of the relative distance ratio. Red line indicates the actual path that the pollen tube takes from transmitting tract to micropyle. Green line indicates the direct distance between transmitting tract and micropyle. The ratio of red line length to green line length gives the relative distance ratio. The relative distance ratios of *map18* and *MAP18 OX* pollen tubes are significantly greater than those of wild-type pollen tubes. Error bars indicate ± SD. ***$P < 0.001$, by Student's t test.

(J) Significant seed gaps are observed in the siliques of *map18* mutants and *MAP18 OX*. This defect is complemented in COM#1 using wild-type Col for comparison. Bar = 1 mm.

(K) Fertilized (green and mature) and aborted unfertilized (thin and barren; asterisks) ovules in dissected siliques. The complementation construct was able to rescue the abortion phenotype in COM#1. Bar = 0.5 mm.

(L) Seed setting rates were analyzed for wild-type, COM#1, *map18*, and *MAP18 OX* siliques. The seed setting rates for both *map18* and *MAP18 OX* were significantly lower than those of wild-type specimens. No significant difference was detected between wild-type and COM#1 seed setting rates. Error bars indicate ± SD. **$P < 0.01$, by Student's t test.

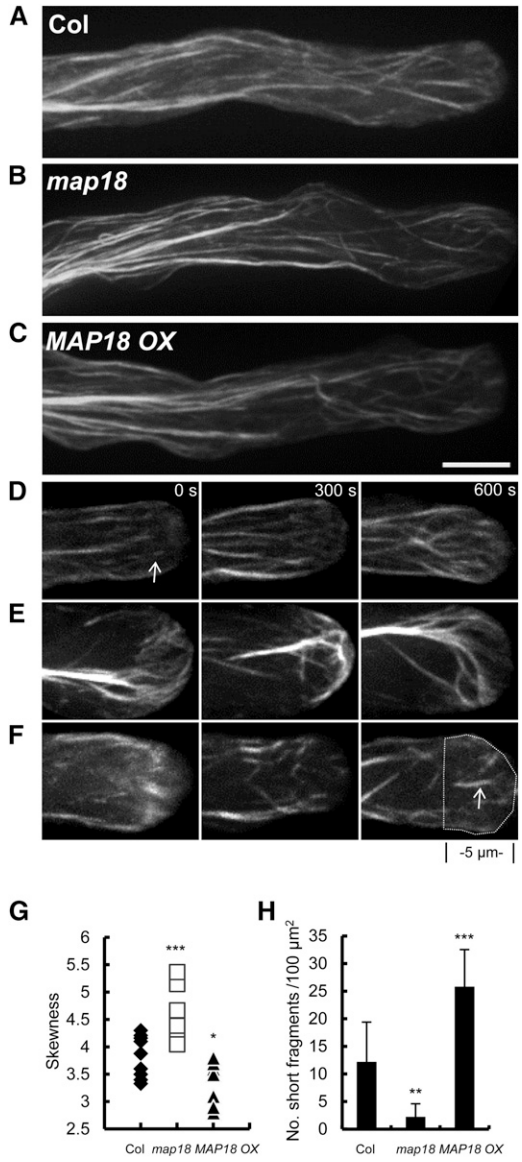

Figure 3. Apical Actin Filaments Are Disorganized, and Actin Cables Protrude into the Extreme Tips of *map18* Pollen Tubes.

(A) to **(C)** Axial actin cables were arranged longitudinally in the shanks of wild-type **(A)**, *map18* **(B)**, and *MAP18 OX* **(C)** pollen tubes.

(D) Time-lapse images taken from Supplemental Movie 1 online, showing that short fine actin filaments existed in the apex of a wild-type pollen tube.

(E) Time-lapse images taken from Supplemental Movie 2 online, showing that in a *map18* pollen tube, actin cables protruded into the apical region, whereas short fine actin filaments were absent.

(F) Time-lapse images taken from Supplemental Movie 3 online, showing that in the apical region of a *MAP18 OX* pollen tube, excessive fine actin structures were observed in a scattered pattern in the tip.

More than 50 pollen tubes were observed from each line. Representative images are presented in **(A)** to **(F)**. Bar in **(C)** = 5 μm for **(A)** to **(F)**.

(G) The bundling of F-actin in apex was increased in *map18* (***$P < 0.001$, Student's *t* test) but decreased in *MAP18 OX* (*$P < 0.05$, Student's *t* test) based on skewness analysis. The skewness values of each pollen tube analyzed are shown ($n = 10$).

supernatant $(MAP18]_{free}$) and the resulting data fitted with a hyperbolic function. In a representative experiment shown in Figure 4C, the K_d was determined to be 0.22 μM. A mean K_d value (±SD) from three independent experiments was 0.26 ± 0.04 μM. As a control, the mean K_d value of VLN2 was determined to be 1.4 ± 0.2 μM ($n = 3$), which is consistent with a previously published value (K_d = 1.3 ± 0.5 μM; Bao et al., 2012).

To test whether GST-MAP18 bound F-actin in vitro, Alexa 488–phalloidin–stabilized F-actin was incubated with recombinant GST-MAP18 and was then stained with an anti-MAP18 primary antibody (Wang et al., 2007) followed by a fluorescent-labeled secondary antibody. Samples were visualized under a microscope equipped with a charge-coupled device (CCD) camera. Recombinant GST-MAP18 localized as punctate structures along F-actin (Figures 4D to 4F). These structures were not detected when GST-MAP18 was first denatured by boiling (Figures 4G to 4I) or when the primary antibody was omitted (Figures 4J to 4L). These results suggest that GST-MAP18 binds to F-actin in vitro.

Next, we analyzed the effect of GST-MAP18 on actin polymerization by monitoring the polymerization of pyrene-labeled actin in the presence of various concentrations of GST-MAP18. The polymerization rate and the quantity of F-actin at equilibrium were unaffected by the presence or absence of GST-MAP18 (see Supplemental Figure 4 online), indicating that GST-MAP18 does not regulate actin polymerization.

MAP18 also been described as PCaP2, owing to its capacity to bind calcium (Kato et al., 2010). Because Ca^{2+} is markedly elevated in the apex of pollen tubes, we speculated that MAP18 could exhibit its activities on F-actin in a Ca^{2+}-dependent manner. We observed actin filaments following incubation with GST-MAP18 in the presence or absence of Ca^{2+}. We detected no change in actin filaments (Figure 4M) when they were incubated with 10 nM GST-MAP18 (Figure 4N) or with 50 μM Ca^{2+} alone (Figure 4O). However, actin filaments were fragmented if GST-MAP18 was present together with 50 μM Ca^{2+} (Figure 4P). These results confirmed that Ca^{2+} is required for MAP18 to sever actin filaments.

Time-lapse total internal reflection fluorescence microscopy (TIRFM) was employed to directly observe the F-actin-severing activity of MAP18. Although few breaks in the Alexa 488–phalloidin–stabilized actin filaments were observed in control samples incubated with either GST-MAP18 or Ca^{2+} alone, the addition of GST-MAP18 induced breaks along the actin filaments in the presence of 50 μM Ca^{2+} over time (Figure 4Q; see Supplemental Movie 4 online). The number of breaks per unit of filament length per second (breaks μm^{-1} s^{-1}) was defined as the severing frequency and was used to characterize the severing activity of MAP18 (Zhang et al., 2010; Zhang et al., 2011). MAP18 significantly raised the severing frequency to 0.0011 ± 0.0002 in the

(H) Quantitative analysis of the number of short F-actin fragments in the apex of pollen tubes (the region was defined as indicated by the dashed line in **[F]**) showed that *MAP18 OX* pollen tubes contained more F-actin fragments that were <2 μm in length than did the wild type. However, this type of F-actin was rarely seen in *map18* pollen tubes.

***$P < 0.001$ and **$P < 0.01$; Student's *t* test. More than 20 growing pollen tubes for each line were quantified and error bars represent ± SD.

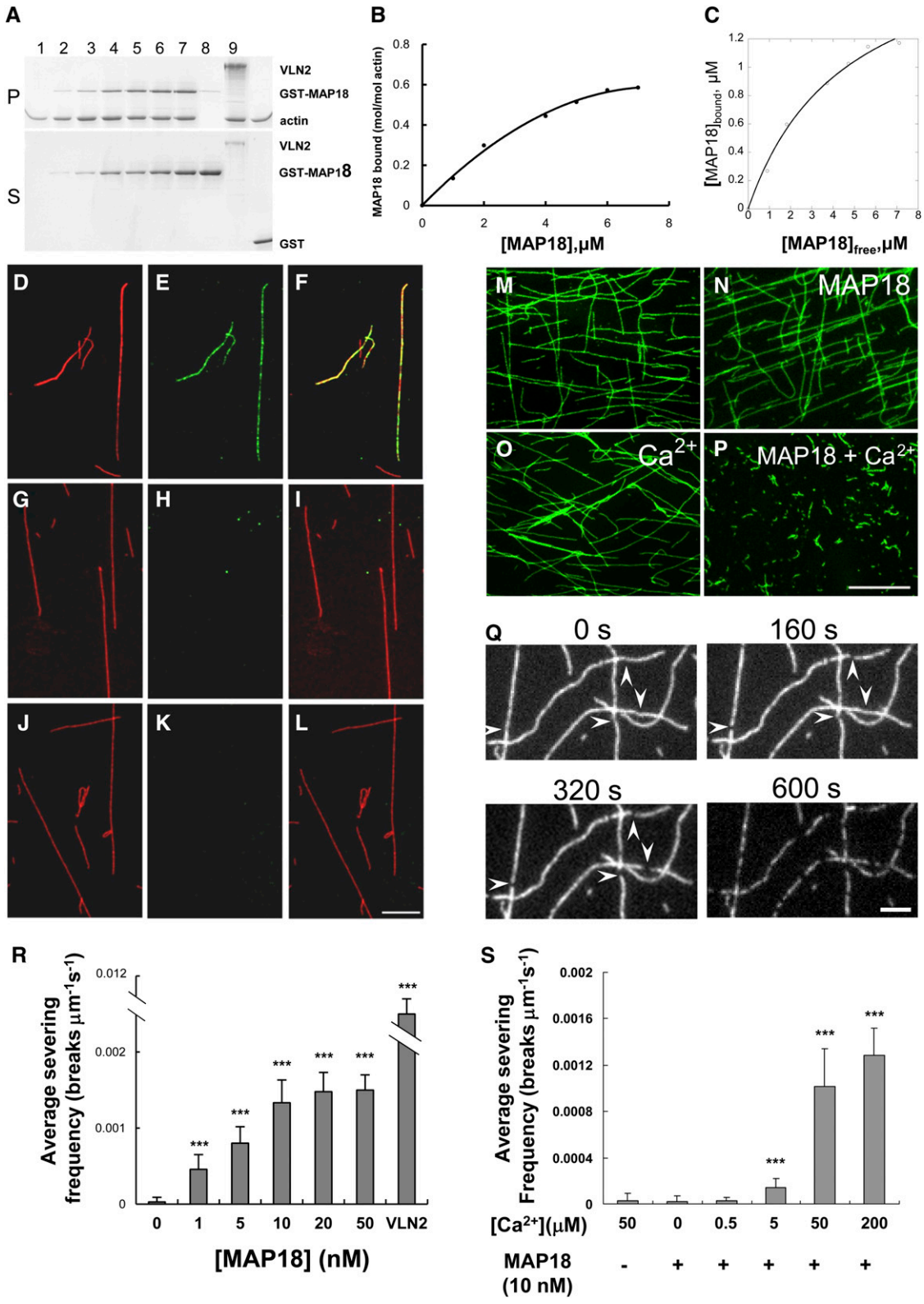

Figure 4. MAP18 Binds to F-Actin and Severs F-Actin in a Ca^{2+}-Dependent Manner in Vitro.

(A) A cosedimentation assay was performed to assess GST-MAP18 binding to actin filaments. Preformed F-actin was incubated with various concentrations of recombinant GST-MAP18. Positive control, VLN2; negative control, GST. GST-MAP18 binds to F-actin in vitro. Lanes 1 to 7, 0, 1, 2, 4, 5, 6, and 7 μM GST-MAP18; lanes 1 to 6, 8, and 9: 2 μM F-actin; lane 8, 3.5 μM VLN2; lane 9, 7 μM GST. Experiments were repeated at least three times and a representative result is shown. P, pellets; S, supernatants.

(B) Densitometry analysis of the results shown in **(A)**. Binding to F-actin is saturated at a stoichiometry of 0.58 mol GST-MAP18 per mol of G-actin.

presence of Ca^{2+}, compared with 0.00002 ± 0.00004 in the absence of Ca^{2+} (Student's *t* test, $P < 0.001$) or 0.00003 ± 0.00006 when F-actin was incubated with Ca^{2+} in the absence of MAP18 ($P < 0.001$). MAP18 severed F-actin in a dose-dependent manner (Figure 4R) and reached saturation when the MAP18 concentration exceeded 10 nM (i.e., we detected no statistical difference between 10 and 20 nM). To rule out the potential negative effects of phalloidin in this assay, we analyzed the severing frequencies of MAP18 under various concentrations of phalloidin, and no significant difference was detected (see Supplemental Figure 5 online). As a control, the average severing frequency of 5 nM VLN2 was 0.011 ± 0.0008. Therefore, there was no negative effect on severing of MAP18 when F-actin was labeled by phalloidin.

To confirm that the severing activity of MAP18 was Ca^{2+} dose dependent, 10 nM MAP18 was incubated with various concentrations of Ca^{2+}. The severing frequency increased with an increase in Ca^{2+} concentration (Figure 4S). No severing activity was detected when the Ca^{2+} concentration was below 0.5 μM; however, the average severing frequency clearly increased when the Ca^{2+} concentration exceeded 5 μM. These findings indicated that GST-MAP18 can sever actin filaments in a Ca^{2+} dose-dependent manner. Interestingly, the F-actin binding of MAP18 was not affected by Ca^{2+}; the mean K_d value of MAP18 was 0.27 ± 0.08 μM in the presence of 1 mM Ca^{2+}, which is quite similar to the mean K_d value of 0.26 ± 0.04 μM in the absence of Ca^{2+}.

Subcellular Localization of MAP18 in Pollen Tubes

Using MAP18-eGFP, we analyzed the localization patterns of MAP18 in pollen tubes during pollen tube growth. At 4 h after germination, the control green fluorescent protein (GFP) signal driven by the *MAP18* promoter in the *map18* background was uniformly distributed throughout the cytoplasm (Figure 5A). In pollen tubes expressing *MAP18-eGFP* (*map18* background), the fluorescence signal was detected primarily at the plasma membrane in the flanks of pollen tubes and in the inverted cones of the apical regions (Figures 5B and 5E). Plasmolysis revealed that MAP18-eGFP was associated with the plasma membrane and not the cell wall (Figure 5D). Cross-sectioning through the Z-stack projection of a pollen tube at the shank region confirmed that MAP18-eGFP was enriched at the plasma membrane (Figure 5B, inset).

We quantified the MAP18-eGFP fluorescence ratio of the membranous-to-cytoplasmic signal in pollen tubes. A line was drawn across the pollen tube shank or across the pollen tube tip, and the fluorescence pixel intensity was measured by ImageJ (Figure 5B). The fluorescence signal ratio was 1.4 in shanks and 0.8 in the apical regions ($P < 0.001$, Student's *t* test). Typical pixel intensities corresponding to the lines in Figure 5B were plotted in Figure 5F. This confirmed that MAP18-eGFP was mainly localized to the shank plasma membrane and the inverted cone of the apex.

When pollen tube growth slowed down occasionally or was arrested by freezing at −20°C for 20 min (Wang et al., 2008), a temporary MAP18-eGFP signal was detected at the apical plasma membrane that disappeared when pollen tube growth resumed (Figure 5C; see Supplemental Figures 6A and 6B and Supplemental Movie 5 online). This plasma membrane location pattern of MAP18 in pollen tubes was confirmed by immunofluorescence microscopy using a previously reported anti-MAP18 polyclonal antibody (Wang et al., 2007) (see Supplemental Figure 7 online).

Taken together, our observation suggested that the association of MAP18 with the apical plasma membrane was related to the ceasing growth of pollen tubes. To maintain pollen tube growth, MAP18 must be removed from the apical plasma membrane.

Figure 4. (continued).

(C) The amount of MAP18 in the pellet (bound) was plotted against the amount of MAP18 in the supernatant (free) and fitted with a hyperbolic function. This experiment was repeated more than three times, and the mean value of the calculated dissociation constant (K_d) was 0.26 ± 0.04 μM. For this representative experiment, the K_d value was 0.22 μM.

(D) to **(L)** In vitro immunofluorescent microscopy demonstrated that GST-MAP18 colocalizes with F-actin. GST-MAP18 was incubated with Alexa 488–phalloidin–stabilized F-actin (pseudocolored red) and was then stained with anti-MAP18 primary antibody and tetramethylrhodamine isothiocyanate–conjugated goat anti-rabbit secondary IgG (pseudocolored green). Bar in **(L)** = 5 μm for **(D)** to **(L)**.

(D), **(G)**, and **(J)** F-actin.

(E) GST-MAP18.

(H) Denatured MAP18.

(K) Secondary antibody alone (negative control).

(F) Merged image of **(D)** and **(E)**.

(I) Merged image of **(G)** and **(H)**.

(L) Merged image of **(J)** and **(K)**.

(M) to **(P)** Preformed actin filaments (labeled with Alexa 488–phalloidin) remain intact when incubated with 10 nM GST-MAP18 **(N)** or 50 μM Ca^{2+} **(O)**. Actin filaments are fragmented in the presence of GST-MAP18 together with 50 μM Ca^{2+} **(P)**. Bar in **(P)** = 10 μm for **(M)** to **(P)**.

(Q) Time-lapse images taken from Supplemental Movie 4 online showing the severing activity of MAP18. TIRFM imaging was started right after the addition of MAP18 and 50 μM Ca^{2+} to the system. Each individual filament displayed an increasing number of breaks (arrowheads) as time elapsed. Bar = 2 μm.

(R) The mean severing frequencies were plotted against the concentration of MAP18 (in the presence of 50 μM Ca^{2+}). MAP18 severs actin filaments in a dose-dependent manner. There is no obvious increase of the severing frequencies when the concentration of MAP18 was over 10 nM. The mean severing frequency of 5 nM VLN2 was used as a positive control. Experiments were repeated at least three times. Each experiment examined more than 15 filaments. Error bars represent ± SD. ***$P < 0.001$ by Student's *t* test in comparison to 0 nM MAP18.

(S) F-actin severing frequencies of 10 nM MAP18 in the presence of various concentrations of Ca^{2+}. Experiments were repeated at least three times. More than 15 filaments were examined for each experiment. Error bars represent ± SD. ***$P < 0.001$ by Student's *t* test in comparison with the control.

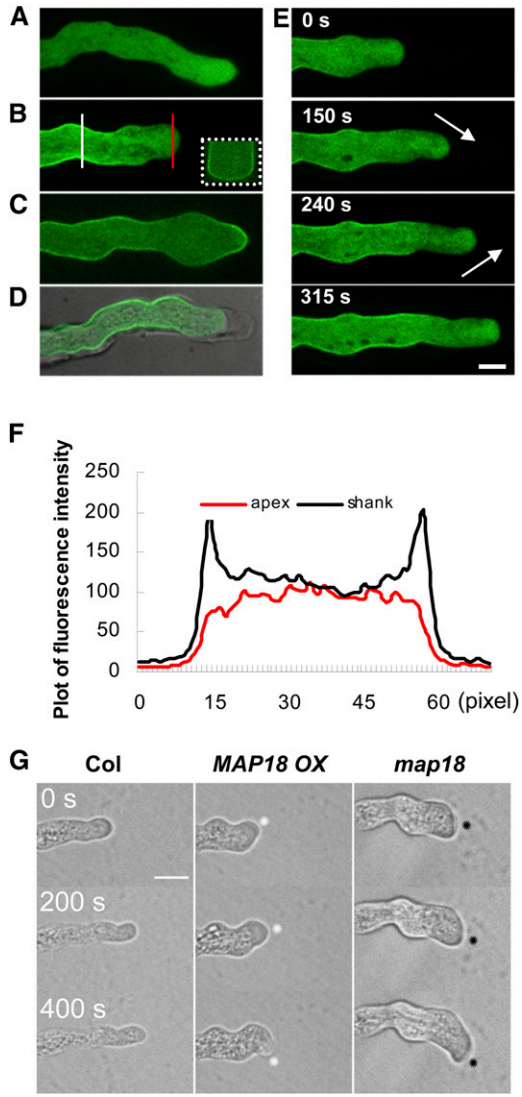

Figure 5. MAP18-eGFP Localizes to the Flank Plasma Membrane of Growing Pollen Tubes.

(A) Mid-plane section of a growing pollen tube expressing eGFP driven by the MAP18 promoter in a *map18* mutant background. GFP exhibits cytosolic distribution.

(B) Mid-plane section of a growing MAP18-eGFP pollen tube in which MAP18-eGFP localizes to the flank plasma membrane and the inverted cone of the apical region. Inset outlined with white dots is a cross section that displays the elevated signal intensity in the surrounding plasma membrane. Cross section is through the Z-stack projection indicated by the solid white line. The red line indicates the position where arbitrary units were measured across the pollen tube tip as in **(F)**.

(C) MAP18-eGFP signal observed at the apical plasma membrane in a nongrowing MAP18-eGFP pollen tube.

(D) MAP18-eGFP pollen tube undergoing plasmolysis exhibits a GFP signal at the shank plasma membrane, but not the cell wall.

(E) Time-course series of a growing pollen tube expressing MAP18-eGFP, showing the subcellular localization of MAP18. MAP18 accumulates primarily in the apical region and the flank plasma membrane near the pollen tube tip. Numbers refer to time intervals. The location of MAP18-eGFP in the inverted cone relocates continuously with the reorienting trajectory of pollen tube growth (arrows). Bar in **(E)** = 10 μm in **(A)** to **(E)**.

(F) Fluorescence intensities (arbitrary units) across the pollen tube shanks (white line) or across the pollen tube tips (red line) in **(B)**. The MAP18-eGFP fusion protein localizes to the plasma membrane at the shank of the growing pollen tube.

(G) Time-lapse images of the growth trajectories of wild-type Col, *MAP18 OX*, and *map18* pollen tubes. The dots indicate the pollen tube growing sites. Images were collected every 5 s. Bar = 20 μm.

Furthermore, in the apical region, the distribution of cytosolic MAP18-eGFP in the inverted cone was continually relocalized to the region of new growth when pollen tubes were reorienting their growth trajectories (Figure 5E). Real-time imaging revealed that the growth rates of *MAP18 OX* and *map18* pollen tubes were similar to that of the wild type (Figure 5G). However, *MAP18 OX* pollen tubes were constantly readjusting their growth directions, exhibiting swinging growth trajectories, whereas *map18* pollen tubes maintained a clockwise bending under the microscope. These findings indicated that MAP18 is important for regulating the directionality of pollen tube growth.

F-Actin-Severing Activity Is Crucial for MAP18 Functioning in Pollen Tube Growth

To further investigate the function of MAP18 in pollen tube directional growth, we generated MAP18 protein mutants by site-directed mutagenesis, in which the Glu (E) or Lys (K) residues in the VEEKK motifs of MAP18 were mutated into Ala or Gly residues (named MAP18-M1 to M7, respectively) (see Supplemental Figure 8 and Supplemental Table 1 online). Six MAP18 protein mutants (M1, M2, M3, M4, M6, and M7) were obtained (see Supplemental Table 2 online). Recombinant mutant proteins were prepared and purified for in vitro analyses. M1 and M2 were unable to sever F-actin in the presence of 50 μM Ca^{2+}, although they still bound F-actin (see Supplemental Table 2 online) with K_d values that were similar to wild-type MAP18 (see Supplemental Figures 9A to 9C online). By contrast, there were no obvious differences in F-actin-severing activities between the other four mutant proteins (M3, M4, M6, and M7) and wild-type MAP18, and all the mutant proteins could bind F-actin in vitro (see Supplemental Figure 9 and Supplemental Table 2 online). Mutants M1 and M2 (lacking F-actin-severing activity in the presence of Ca^{2+}) and M7 (maintaining F-actin-severing activity in the presence of Ca^{2+}) were chosen for further phenotypic observations and functional analyses.

Each MAP18 mutant (M1, M2, and M7) was fused with eGFP and introduced into *map18* plants under the control of *MAP18* promoter, respectively. Lines expressing MAP18 mutant proteins to a level that is comparable to the expression level of MAP18 in wild-type plants were chosen for further analysis (named *m1*, *m2*, and *m7*, respectively; see Supplemental Figure 10 online).

Pollen tubes *m1* and *m2* germinated in vitro exhibited no obvious defects in elongation (Figure 6A) and displayed the bending growth pattern characteristic of *map18* pollen tubes. By contrast, *m7* pollen tubes reduced the growth bending angle to a level that mimicked wild-type tubes, thereby compensating for the *map18* phenotype (Figure 6B).

We subsequently investigated pollen tube growth in the stigma and style. Similar to *map18* pollen tubes, *m1* and *m2* pollen tubes exhibited aberrant growth patterns (Figure 6C). However, *m7* pollen tubes grew relatively normally in pistils, indicating that *m7* complemented *map18*. Quantification and statistical analysis indicated that the relative distance ratios of *m1* (1.9 ± 0.7, *n* = 28) and *m2* (2.0 ± 0.6, *n* = 20) were greater than those of wild-type (1.3 ± 0.3, *n* = 48) and *m7* (1.3 ± 0.2, *n* = 31) pollen tubes ($P < 0.001$, Student's *t* test), whereas no significant differences between wild-type and *m7* pollen tubes were observed ($P = 0.8$, Student's *t* test) (Figure 6C, inset). Moreover, the overall number of seeds in siliques was reduced substantially in *m1* and *m2*, but not in *m7*, in comparison to the wild type (Figures 6D and 6E).

We also examined the subcellular distributions of these three mutant proteins. Green fluorescence of M1-eGFP, M2-eGFP, or M7-eGFP was detected on the flank plasma membranes and in the inverted cones of the apical regions of growing pollen tubes, similar to wild-type MAP18-eGFP (COM#1) (Figure 6F). These observations indicated that the subcellular localization of MAP18 was not altered with these protein mutations. Therefore, the effects on pollen tube growth and fertilization events observed in *m1*, *m2*, and *m7* mutants were likely due to their various F-actin-severing activities and not their subcellular distributions. In addition, we observed the localization patterns of MAP18-eGFP, M1-eGFP, M2-eGFP, and M7-eGFP in root epidermal cells using immunofluorescence microscopy. As nontagged wild-type MAP18 recognized by anti-MAP18 antibody, GFP-tagged MAP18 and its

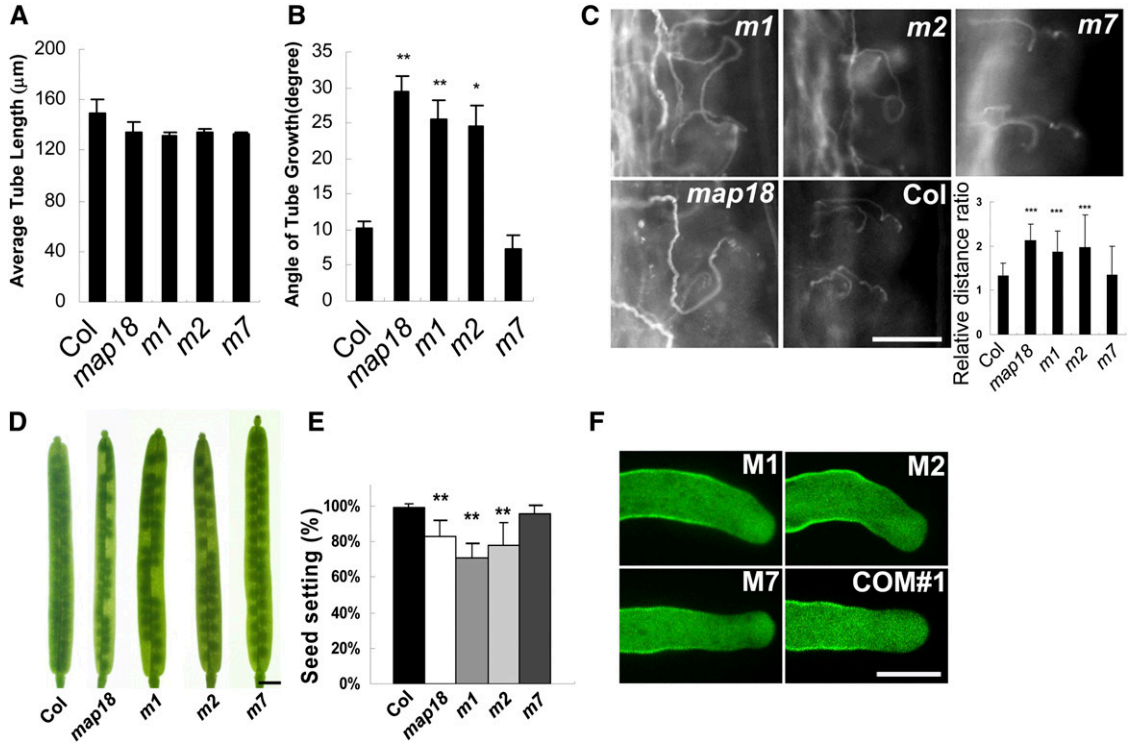

Figure 6. Phenotype Analyses of Pollen Tubes and Siliques Expressing MAP18 Mutant Proteins.

Arabidopsis lines expressing eGFP-tagged MAP18 mutant proteins driven by the *MAP18* promoter in a *map18* background were generated and named *m1*, *m2*, and *m7*.

(A) At 4 h after germination, average pollen tube lengths were determined. The *m1*, *m2*, and *m7* pollen tubes were statistically similar in length to the wild-type pollen tubes.

(B) Measurements of the angles of growing tubes indicate that *m1* and *m2* pollen tubes display bending degrees that are similar to *map18*. However, the bending angles of growing *m7* pollen tubes were reduced relative to those of wild-type tubes. Results were obtained from >60 pollen tubes in each line. Error bars represent ±SD based on three independent experiments. **$P < 0.01$ and *$P < 0.05$ by Student's *t* test.

(C) Aniline blue staining of pollen tube growth for *m1*, *m2*, and *m7* specimens in vivo. The *m1* and *m2* pollen tubes displayed abnormal growth patterns similar to the *map18* pollen tubes. This defect was barely observed in *m7* or wild-type samples. The relative distance ratios for *m1* and *m2* were greater than those for wild-type and *m7* pollen tubes. Error bars show ±SD. ***$P < 0.001$ by Student's *t*-test. Bar = 100 μm.

(D) Seed gaps are observed in *m1* and *m2* siliques, but not in *m7* siliques. Bar = 1 mm.

(E) Seed setting analysis of wild-type, *map18*, *m1*, *m2*, and *m7* mutant siliques. Total seeds are reduced significantly in *m1* and *m2* siliques, but not in *m7* siliques, in comparison with the wild type. Error bars indicate ±SD; **$P < 0.01$ by Student's *t* test.

(F) M1-eGFP, M2-eGFP, and M7-eGFP localize to the flank plasma membranes and the characteristic inverted cones of the apical regions of growing pollen tubes, similar to the wild-type form of MAP18-eGFP (COM#1). However, only M7 can rescue the bending growth phenotype. Bar = 10 μm.

[See online article for color version of this figure.]

mutant proteins were still partially colocalized with cortical microtubules in root cells (see Supplemental Figure 11 online). This further demonstrated the plasma membrane localization pattern of MAP18 and MAP18 mutant proteins in pollen tubes was not an artifact caused by GFP tagging.

Together, we conclude that the function of MAP18 in modulating F-actin is crucial for pollen tube growth.

DISCUSSION

MAP18 Is Involved in the Regulation of Pollen Tube Growth Direction

Pollen tubes grow under the guidance of the female reproductive tissues and enter into the ovule via the micropyle for fertilization (Hulskamp et al., 1995). What factors control the direction of pollen tubes is an important research question (Justus et al., 2004; Cárdenas et al., 2005; Coelho and Malhó, 2006; Gossot and Geitmann, 2007; Bou Daher and Geitmann, 2011).

Although we detected *MAP18* expression in pollen tubes, we observed no obvious differences in germination or pollen tube elongation rates between wild-type and *map18* mutants. This suggested that *MAP18* might not function in these processes. However, in vitro–germinated *map18* pollen tubes did display abnormal growth patterns, with swollen tips and bending growth. In addition, in vivo analyses indicated that *map18* pollen tubes exhibited aberrant growth in pistils, with extensive meandering pollen tube growth patterns around the micropyles. *MAP18 OX* pollen tubes also displayed entangled, sporadic growth patterns toward the transmitting tracts, sometimes failing to reach the ovules. Both *map18* and *MAP18 OX* pollen tubes showed reduced micropyle targeting in vivo. Similar phenotypes have been observed with *Arabidopsis* pollen-expressed Rab GTPase RabA4d, which localizes to the tips of growing pollen tubes and regulates tip growth. The *raba4d* mutant pollen tubes display a wavy growth pattern in vitro and aberrant growth in the ovary with reduced guidance toward the micropyle (Szumlanski and Nielsen, 2009). Tobacco (*Nicotiana tabacum*) pollen-expressed Rab11b also localizes predominantly to the apical clear zone of elongating pollen tubes. The proper regulation of Rab11b GTPase activity is essential for tip-focused membrane trafficking, pollen tube growth rate, directionality, and male fertility. Transformed pollen tubes expressing GFP-Rab11b (DN) or GFP-Rab11b (CA) displayed dramatic twists, turns, and meandering phenotypes, compromising their ability to direct their growth trajectories toward the micropyle (de Graaf et al., 2005). These reports support an association between wavy or curvy pollen tube growth patterns and defects in male fertility.

F-Actin-Severing Activity and the Direction of Pollen Tube Growth

F-actin plays important roles in many aspects of plant cell development. A large group of ABPs regulate the organization and dynamics of F-actin by their severing, capping, bundling, or cross-linking activities (Staiger, 2000). Recently, the F-actin-severing activity of several ABPs, including ADF4 and CP, was demonstrated in living plant cells (Henty et al., 2011; Li et al., 2012). These F-actin-severing proteins are involved in the regulation of axial expansion of hypocotyl epidermal cells through facilitating the dynamic turnover of F-actin (Staiger et al., 2009). ABPs with F-actin-severing activity have been identified in pollen tubes as well. ADFs and villin superfamily proteins depolymerize F-actin to maintain the dynamics and balance of actin in the subapical and apical region of growing pollen tubes, thereby promoting normal pollen tube growth (Chen et al., 2002; Cheung et al., 2008; Daher and Geitmann, 2012). *Arabidopsis* VLN3 and VLN5 are capable of severing actin filaments and regulating pollen tube growth (Khurana et al., 2010; Zhang et al., 2010); however, it is largely unknown if severing F-actin is relevant to the control of pollen tube growth direction. In this study, we analyze MAP18 mutants expressing various point mutations to demonstrate that the F-actin-severing activity of MAP18 is important for appropriate growth patterns of *Arabidopsis* pollen tubes. The *m1* and *m2 Arabidopsis* lines expressing M1 and M2 (MAP18 mutant proteins specifically lacking F-actin-severing activity), respectively, in a *map18* background displayed phenotypes similar to *map18*. However, the *m7* line expressing M7 protein (a MAP18 mutant protein that retained F-actin-severing activity) in a *map18* background exhibited reduced bending growth compared with *map18* and the transgene complemented *map18* phenotypes, including extension of the meandering pollen tube around the micropyles, unfertilized ovules, and reduced seed setting. Therefore, we propose that MAP18 plays a crucial role in the regulation of growth direction of pollen tubes in *Arabidopsis*, most likely through its F-actin-severing activity.

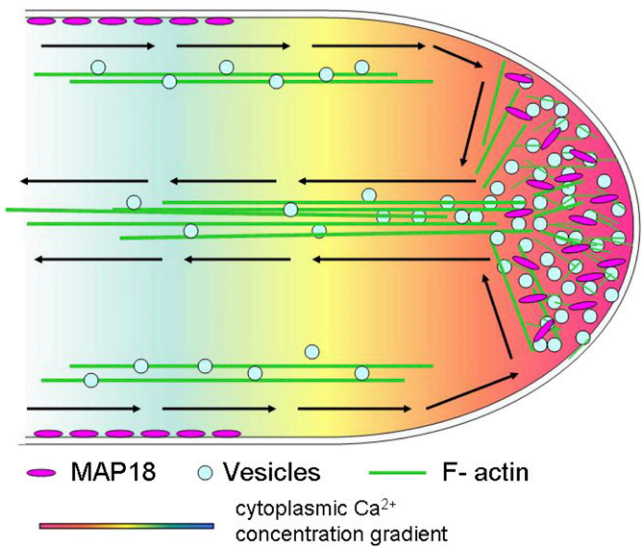

Figure 7. Model Depicting the Function of MAP18 in Pollen Tube Growth Direction.

Schematic diagram of a growing pollen tube with rainbow shading representing the tip-focused [Ca^{2+}] gradient. Actin cables of the shank run parallel to the direction of growth. MAP18 dominantly binds to the plasma membrane at the shank. The high cytosolic calcium level in the apical region results in increased cytosolic MAP18, which severs actin filaments. This remodels actin organization in the apex to regulate pollen tube growth direction such that pollen tubes can appropriately target ovules for fertilization.

F-Actin-Severing Activity of MAP18 and Calcium

There is a close relationship between intracellular Ca^{2+} and the cytoskeleton in the pollen tube apex, where ion fluxes, operating through different ABPs, regulate the structure and activity of F-actin (Cárdenas et al., 2008). In this study, we determined that the F-actin-severing activity of MAP18 is Ca^{2+} dependent. This dependence is particularly interesting, considering that a calcium gradient exists in the pollen tube tip. It is likely that the F-actin-severing activity of MAP18 is limited to the apical region of the pollen tube where an exclusively localized, high concentration of Ca^{2+} exists.

Other ABPs with Ca^{2+}-dependent F-actin-severing activity are involved in pollen tube growth. For instance, *Arabidopsis* VLN2, VLN3, and VLN5 are capable of severing actin filaments in a Ca^{2+}-dependent manner. VLN3 bundles actin filaments independently of Ca^{2+} but severs filaments in the presence of micromolar [Ca^{2+}] (Khurana et al., 2010). Biochemical analyses showed that VLN2 was able to sever actin filaments in a similar manner to VLN3 (Bao et al., 2012). VLN5 is a major actin-filament-stabilizing factor and a regulator of actin dynamics that functions in concert with oscillatory Ca^{2+} gradients and is essential for pollen germination and tube growth (Zhang et al., 2010). We showed that the activity of MAP18 on actin filaments depends strictly on calcium. MAP18 exhibited no effects on actin filaments in the absence of Ca^{2+} but severed actin filaments in the presence of Ca^{2+}. Thus, the severing activity of MAP18 could proceed in the apical region without affecting actin cables in the shank.

Although our results demonstrated that the F-actin-severing activity of MAP18 depends on Ca^{2+} in vitro, we were unable to confirm this in pollen tubes due to technical problems. The tip-focused Ca^{2+} gradient in *Arabidopsis* pollen tubes is difficult to manipulate with pharmacological treatments, such as A23187 or $LaCl_3$. Therefore, future studies are warranted to determine how the F-actin-severing activity of MAP18 is regulated by Ca^{2+} in live cells.

The Location of MAP18 Is Important for Pollen Tube Growth

In this study, we showed that MAP18 localizes to the plasma membrane, particularly in the flank region of growing pollen tubes. However, MAP18 preferentially localized to the apical plasma membrane in nongrowing pollen tubes and disappeared from the apical plasma membrane when tube growth was restarted. MAP18 in the apical inverted cone continuously relocalized as the growth axis direction of the tube reoriented. In addition, in *MAP18 OX* pollen tubes, MAP18 accumulated in pollen tube tips and frequently changed its location; this phenomenon is associated with the wavy growth phenotype.

Proteins that localize to the subapical plasma membrane are essential for the endocytosis and exocytosis processes that promote and sustain growth. In *Arabidopsis*, phosphatidylinositol-4-monophosphate 5-kinase 4 (PIP5K4)-GFP and PIP5K6-GFP exhibit the same localization shift to the extreme apex in pollen tubes that cease elongation (Sousa et al., 2008; Zhao et al., 2010).

Therefore, we conclude that the distinct localization pattern of MAP18 is important for the directionality of pollen tube tip growth. The dynamic localization of MAP18 in the flank plasma membrane and in the apical cone of the growing pollen tube focuses the growth site to the extreme apex of the growing tip.

The Effect of MAP18 on Microtubules versus F-Actin

We reported previously that MAP18 binds microtubules (Wang et al., 2007). In this study, we demonstrate that MAP18 possesses F-actin-severing activity that is dependent on Ca^{2+}. This suggests that MAP18 may play a role in coordinating the microtubule and actin cytoskeletons.

Proteins interacting with both microtubules and F-actin have been reported in plants (Petrásek and Schwarzerová, 2009). For instance, the CLIP-associated proteins, a group of microtubule plus end–tracking proteins, interact with actin directly and function as actin/microtubule cross-linkers in interphase cells (Tsvetkov et al., 2007). Formins (actin-nucleating proteins) may interact through specific domains with both actin and microtubules (Young et al., 2008; Deeks et al., 2010; Li et al., 2010).

The microtubule-associated protein SB401 from *Solanum berthaultii* contains three CKII phosphorylation sites. It binds and bundles both microtubules and F-actin in vitro and colocalizes with cortical microtubules in pollen tubes (Huang et al., 2007). Its bundling activity requires the formation of dimers and is regulated by phosphorylation that decreases its affinity to microtubules without influencing its F-actin bundling activity (Liu et al., 2009). Regulation by phosphorylation also is found in other proteins that bind both microtubules and F-actin. MAP1B binds microtubules and F-actin; phosphorylation specifically abrogates its ability to bind F-actin (Gordon-Weeks and Fischer, 2000; Mack et al., 2000; Riederer, 2007). MAP18 contains potential phosphorylation sites as predicted using the NetPhos 2.0 program (http://www.cbs.dtu.dk/services/NetPhos/) (Kato et al., 2010). Therefore, we hypothesized that phosphorylation of MAP18 might affect its effect on microtubules. MAP18 contains seven repeated motifs of VEEKK (Wang et al., 2007); these repeats are also found in SB401 and MAP1B sequences.

Conversely, our observations showed that the F-actin-severing activity of MAP18 depends on tip-focused Ca^{2+} in pollen tubes, and the localization of MAP18 on the plasma membrane might be affected by calcium. Therefore, calcium may be a key regulator of the MAP18-mediated reorganization of the actin cytoskeleton.

We propose a model for the function of MAP18 in pollen tube growth (Figure 7). MAP18 dominantly binds to the plasma membrane at the shank. Elevated levels of cytosolic calcium in the apical region result in increased levels of cytosolic MAP18, which severs actin filaments. This process remodels actin in the apex to guide the growth direction of the pollen tube so that pollen tubes can properly target ovules for fertilization.

METHODS

Plant Material and Growth Conditions

Arabidopsis thaliana ecotype Col was the background for all wild-type and mutant tissues described in this study. Plants were grown in soil at 22°C with a photoperiod of 16 h light/8 h dark. Seeds were sterilized for 15 min in 0.5% sodium hypochlorite and then were immersed in growth medium at 4°C in the dark for 2 d before transferring to the growth room. An *Arabidopsis* line expressing *Lat52:lifeact-mEGFP* was crossed to the *map18* mutant and *MAP18 OX*, *m1*, *m2*, and *m7* transgenic plants (see below). Lines that displayed a similar fluorescence intensity under the same microscopy settings were chosen for further analysis (see Supplemental

Figure 12 online). The growth medium contained half-strength Murashige and Skoog salts and 0.9% Phytagel (Sigma-Aldrich).

Verification of *MAP18* T-DNA Insertion Lines

Arabidopsis lines (Col background) with T-DNA insertions in *MAP18* were obtained from the ABRC (*map18*, SALK_021652). A PCR-based approach was used to identify homozygous lines. PCR genotyping was performed using three primers: a primer near the right border of the T-DNA insert (LBb1, 5′-GCGTGGACCGCTTGCTGCAACT-3′) and a pair of *MAP18*-specific primers (*MAP18*-LP, 5′-TGATTTCCTTTAAATAGCCAGAGTG-3′, and *MAP18*-RP, 5′-AAAAACAAGGCAGGATCATCG-3′). Homozygous lines were used in subsequent analyses.

qRT-PCR analysis was performed to test whether *map18* homozygous plants generated *MAP18* transcripts. Total RNA was extracted from inflorescences and flowers using TRIzol reagent (Invitrogen) according to the manufacturer's instructions. The coding region of *MAP18* was amplified by qRT-PCR using the following primer set: *MAP18* forward, 5′-AAGCCAGCTGTGGAAGA-3′, and reverse, 5′-TTCGGGAGCCTTAGT-3′. As a positive control, *EF1*α transcript levels were measured in the same tissues using the primer set: *EF1*α forward, 5′- ACGCTCTTCTTGCTTTCACC-3′, and *EF1*α reverse, 5′-GAGATTGGCACAAATGGGAT-3′. SYBR Premix Ex Taq (Takara Bio) was used for amplification.

Plasmid Construction and Plant Transformation

The plant transformation vector pCAMBIA1390 (Cambia) was used to generate transformed plants. A 2.2-kb region of the *MAP18* promoter was amplified from wild-type genomic DNA using the primers 5′-AAGCTTACGAGTGACTCAACTCCTCTCCA-3′ and 5′-CCCGGGGGATCCGTCGACCTTTTAAAAAATTAACCTGCCACC-3′, as previously described (Wang et al., 2007). The product was cloned into the pCAMBIA1390 vector and used to control the expression of various MAP18-eGFP reporter constructs. MAP18 was amplified using the primers 5′-GTCGACATGGGTTATTGGAAGTC-3′ and 5′-CGGATCCACCACCTCCACCTCCAGCCTTTTGTGGCGCAG-3′, as reported previously (Wang et al., 2007), and eGFP was amplified from the pEZS-NL vector using the primers 5′-CGGATCCATGGTGAGCAAGGGCGAGGA-3′ and 5′-CCCGGGTTACTTGTACAGCTCGTCCATGCCG-3′. Both amplicons were then cloned into the pCAMBIA-*MAP18pro* vector with eGFP at the C terminus.

PCR-based site-directed mutagenesis was performed according to the manufacturer's instructions (MutanBEST; TaKaRa) using a pMD18-*T-MAP18* construct (TaKaRa) as a template. Primer pairs were synthesized that specified the insertion of Ala or Gly within the amino acid residues indicated (see Supplemental Table 1 online). The altered cDNAs were subcloned into pGEX-4T vectors for expression in *Escherichia coli* strain BL21 or into pCAMBIA1390 vectors driven by the native *MAP18* promoter for transformation into *Arabidopsis*. All cDNAs were sequence verified.

Recombinant proteins were expressed and purified as described previously (Wang et al., 2007). Plants were transformed using the *Agrobacterium tumefaciens* strain GV3101 by the floral dip method (Clough and Bent, 1998).

Homozygous *map18* mutant plants were transformed with the pCAMBIA-*MAP18pro*:*MAP18-eGFP* construct for complementation of *map18* plants. Transgenic plants were selected on Murashige and Skoog culture medium containing 30 mg/L hygromycin.

Assays of Pollen Tube Germination and Seed Rate Counting

Arabidopsis pollen grains were germinated on medium consisting of 5 mM MES (pH 5.8, adjusted with Tris), 18% Suc, 1 mM KCl, 5 mM $CaCl_2$, 0.8 mM $MgSO_4$, 1.5 mM boric acid, 0.05% (w/v) lactalbumin hydrolysate, 10 mM myoinositol, and 0.7% (w/v) agarose in a humid chamber, as previously reported (Fan et al., 2001). To achieve plasmolysis, 25% mannitol in liquid germination medium was added to the pollen tube growth culture for 20 min. Approximately 4 h after germination, images of pollen tubes were captured using a BX51 microscope (Olympus) equipped with a CoolSNAP HQ CCD camera (Photometrics) using MetaMorph (Universal Imaging). Pollen tube lengths and growth angles were measured using ImageJ software (National Institutes of Health; http://rsb.info.nih.gov/ij). All experiments were performed in triplicate, and 150 pollen tubes were measured in each experiment.

To evaluate fertilization, seed setting rates were counted in mature siliques to identify unfertilized ovules. Samples were visualized using an Olympus SZX16 microscope equipped with a color CCD camera (Olympus DP70) and ImagePro software (Media Cybernetics).

In Vivo Pollen Tube Staining

Pollen tubes in pistils were stained with aniline blue, as described previously (Wu et al., 2010). Briefly, preemasculated mature flowers were pollinated with wild-type, *MAP18 OX*, or *map18* pollen. After 2 or 24 h, pollinated pistils were incubated in fixative solution (ethanol:acetic acid [v/v] =3:1) for at least 2 h and then in 8 M NaOH softening solution overnight. Samples were then stained with aniline blue solution in the dark. Samples were observed using an Olympus BX51 fluorescence light microscope with $\times$10 to $\times$20 objectives. The UV excitation wavelength maximum was 350 nm, and the emission spectra were collected from 440 to 612 nm.

Spinning Disc Confocal Microscopy and Quantitative Analyses

All fluorescence images of pollen tubes were recorded by spinning disc confocal microscopy (Yokogawa) using an IX81 microscope (Olympus) equipped with an iXon CCD camera (Andor Technology) and a $\times$100 1.45–numerical aperture objective (or a $\times$60 1.42–numerical aperture objective; both Olympus). Images were acquired using iQ software (Andor). GFP was excited using 488-nm argon lasers, and emission was collected through 525 $\pm$ 5.5-nm filters.

To investigate MAP18-eGFP localization, time-lapse images were acquired using 30% laser intensity and operating in the mode 512 $\times$ 512 with an exposure time of 200 ms. Images were captured for 15 min at 5-s intervals.

To observe F-actin organization, Z-stacks of pollen tubes expressing *Lat52:lifeact-mEGFP* (Riedl et al., 2008; Vidali et al., 2009) were obtained, and three-dimensional projections were generated as the final images. Time-lapse images were taken at 30-s intervals over a 10-min period using 150-ms exposure times.

Imaris software (Bitplane) was used to obtain cross sections of pollen tubes from the Z-stacks.

Skewness and density were measured to quantify the extent of F-actin (or microtubule) bundling and the percentage of occupancy of F-actin (or microtubules) in cells as previously described (Higaki et al., 2010; Li et al., 2012). Data were analyzed in ImageJ software (http://rsbweb.nih.gov/ij/; version 1.38).

Immunostaining in Plant Cells

Arabidopsis pollen grains were germinated on solid germination medium at room temperature for 4 h and were stained as previously described (Yu et al., 2009; Cai et al., 2011) with several modifications. Briefly, pollen tubes were immersed in fixative solution (4% paraformaldehyde, 1 mM $MgCl_2$, 1 mM EGTA, 10% Suc, and 100 mM PIPES buffer, pH 6.9) for 90 min and then were washed gently with PBS buffer three times. Fixed pollen tubes were treated with digestion buffer (1% cellulose and 0.5% pectinase in PBS buffer) at room temperature for 45 min and then were washed gently with PBS containing 0.1% Nonidet P-40 three times for 10 min per wash. Mouse anti-α-tubulin monoclonal antibody (Sigma-Aldrich) was diluted 1:600 in liquid germination medium containing 5% Gly and was applied as the primary antibody. Alexa 488–conjugated (or fluorescein isothiocyanate–conjugated) goat anti-mouse IgG (diluted

1:400) was used as the secondary antibody. Pollen tubes were incubated in primary antibody at 4°C overnight and then were incubated in secondary antibody at 37°C in germination medium for 2 h.

Immunofluorescence staining of microtubules or MAP18 and its mutant proteins in root epidermal cells was conducted as previously reported by Wang et al. (2007).

F-Actin Binding Assay

Cosedimentation experiments were performed to test the ability of GST-MAP18 to bind F-actin. All proteins were centrifuged at 100,000*g* for 30 min at 4°C before use. Actin was polymerized at 28°C for 30 min in KMEI buffer (50 mM KCl, 1 mM $MgCl_2$, 1 mM EGTA, and 10 mM imidazole-HCl, pH 7.0). Preformed F-actin (polymerized from 2 μM G-actin) was then incubated with various concentrations of GST-MAP18 (0, 1, 2, 4, 5, 6, and 7 μM; reaction volume 100 μL) at 4°C for 30 min. Following incubation, samples were centrifuged at 100,000*g* for 20 min at 4°C. Aliquots of the supernatant and pellet were analyzed by SDS-PAGE using 10% acrylamide gels. To determine apparent equilibrium dissociation constant (K_d) values, the amount of MAP18 or VLN2 in the pellet and supernatant was analyzed by ImageJ software. A K_d value for MAP18 or VLN2 bound to actin filaments was calculated by fitting a hyperbolic function to the data from plots of protein in the pellet as a function of protein in the supernatant using Kaleidagraph v4.0 software (Synergy Software) according to Wu et al. (2010)

In vitro immunofluorescence labeling was performed to demonstrate MAP18 binding to F-actin. Preformed F-actin was stabilized with Alexa 488-phalloidin (1:1) and was then incubated with recombinant GST-MAP18 at a molar ratio of 50:1 in KMEI buffer at room temperature for 20 min. Anti-MAP18 antibody (1:100) was then added, and samples were incubated at room temperature for 1 h, followed by incubation with tetramethylrhodamine isothiocyanate–conjugated goat anti-rabbit IgG (1:200) at room temperature for 15 min. Aliquots (1 μL) were transferred to slides pretreated with poly-L-Lys. MAP18 denatured by boiling for 2 min or by incubating with secondary antibody alone were used as negative controls. Samples were visualized under a BX51 microscope (Olympus) equipped with a CoolSNAP HQ CCD camera (Photometrics). Images were acquired using MetaMorph 6.0 (Universal Imaging).

The time course of actin polymerization was monitored as reported previously (Huang et al., 2003). Briefly, 3 μM G-actin containing 5% pyrenyl-actin was polymerized in KMEI buffer with various amounts of MAP18 (0, 0.5, 1, 2, and 3 μM). Pyrenyl fluorescence was measured using an F-4500 fluorescence spectrofluorometer (Hitachi). All experiments were performed at least in triplicate under identical conditions.

Assay for F-Actin-Severing Activity of MAP18

To visualize the F-actin-severing activity of MAP18, perfusion cell chambers (~10-μL volumes) were prepared by adhering cover slips to slides with double-sided tape. Chambers were flushed for 10 min with 2 μg/mL poly-L-Lys, washed with Tris-HCl buffer, pH 7.0, and perfused with Alexa 488–phalloidin–labeled F-actin for 3 min to allow the F-actin to bind firmly to the cover slip surface. Chambers were then washed twice with Tris-HCl buffer. Purified GST-MAP18 protein (10 nM) was incubated with 50 mM $CaCl_2$ in 10 mM Tris-HCl buffer for 10 min before being introduced into the perfusion chamber. Time-series images were collected every 20 s by TIRFM (Li et al., 2011). Denatured MAP18 was introduced into the perfusion chamber as a negative control.

Accession Numbers

Sequence data from this article can be found in GenBank/EMBL or the Arabidopsis Genome Initiative databases under accession numbers NC_003076.8 or At5g44610, respectively, for *Arabidopsis MAP18*.

Supplemental Data

The following materials are available in the online version of this article.

Supplemental Figure 1. *MAP18* Expression in Pollen and Pollen Tubes.

Supplemental Figure 2. Pollen Tube Growth Patterns Correlate with MAP18-eGFP Expression.

Supplemental Figure 3. Immunofluorescent Labeling of Microtubules in Pollen Tubes.

Supplemental Figure 4. Recombinant GST-MAP18 Has No Influence on Actin Polymerization.

Supplemental Figure 5. Phalloidin Has No Negative Effect on F-Actin Severing Activity of MAP18.

Supplemental Figure 6. The Association of MAP18 with the Apical Plasma Membrane Is Related to the Cessation of Pollen Tube Growth.

Supplemental Figure 7. Immunostaining by Anti-MAP18 Antibody Confirms the Plasma Membrane Localization Pattern of MAP18.

Supplemental Figure 8. PCR-Based Site-Directed Mutagenesis.

Supplemental Figure 9. F-Actin-Binding and -Severing Activities of MAP18 Mutant Proteins M1, M2, and M7.

Supplemental Figure 10. The qRT-PCR Analysis of the Transcript Levels of *MAP18* and *M1*, *M2*, and *M7* in Various Transgenic Lines.

Supplemental Figure 11. Immunofluorescence Microscopy Demonstrated That GFP-Tagged MAP18 and Its Mutants (M1, M2, and M7) Localized to Microtubules in Root Epidermal Cells.

Supplemental Figure 12. The Relative Fluorescence Intensity of Lifeact-mEGFP Probes in Various Plants.

Supplemental Table 1. Mutated Positions and Primer Information for Seven Site-Directed Mutants of MAP18.

Supplemental Table 2. F-Actin-Binding and -Severing Activities of the Six MAP18 Protein Mutants.

Supplemental Movie 1. Actin Filament Dynamics in a Growing Wild-Type Pollen Tube.

Supplemental Movie 2. Actin Filament Dynamics in a Growing *map18* Pollen Tube.

Supplemental Movie 3. Actin Filament Dynamics in a Growing *MAP18 OX* Pollen Tube.

Supplemental Movie 4. Time-Lapse Series of Actin Filament Severing Following the Addition of 10 nM GST-MAP18 in the Presence of 50 μM Ca^{2+}.

Supplemental Movie 5. MAP18 Associates with the Apical Plasma Membrane When Pollen Tube Growth Slows or Stops.

ACKNOWLEDGMENTS

We thank Shanjin Huang (Institute of Botany, Chinese Academy of Sciences, China) for providing *Arabidopsis* seeds expressing *Lat52*:*lifeact-mEGFP* and for recombinant VLN2 protein. The ABRC provided T-DNA insertion lines. This research was supported by grants from the National Basic Research Program of China (2012CB114200 to Y.F. and M.Y.) and the Natural Science Foundation of China (30721062 and 30830058 to M.Y., 30970173 to L.Z., and 90817105 to Y.F.).

AUTHOR CONTRIBUTIONS

L.Z. and Y.F. designed the project. Y.Z., E.K., and L.Z. performed the experiments and analyzed the results. M.W. designed the site-directed

mutagenesis mutant, and Q.X. generated mutant proteins and performed biochemical analysis. Y.R. performed the plasmid construction. B.L. conducted the pyrene-labeled actin polymerization assay. L.Z. and Y.F. wrote the article. Y.F. and M.Y. revised and modified the article.

Received February 7, 2013; revised February 7, 2013; accepted February 18, 2013; published March 5, 2013.

REFERENCES

Bao, C., Wang, J., Zhang, R., Zhang, B., Zhang, H., Zhou, Y., and Huang, S. (2012). *Arabidopsis* VILLIN2 and VILLIN3 act redundantly in sclerenchyma development via bundling of actin filaments. Plant J. **71:** 962–975.

Bou Daher, F., and Geitmann, A. (2011). Actin is involved in pollen tube tropism through redefining the spatial targeting of secretory vesicles. Traffic **12:** 1537–1551.

Cai, G., and Cresti, M. (2009). Organelle motility in the pollen tube: A tale of 20 years. J. Exp. Bot. **60:** 495–508.

Cai, G., Faleri, C., Del Casino, C., Emons, A.M., and Cresti, M. (2011). Distribution of callose synthase, cellulose synthase, and sucrose synthase in tobacco pollen tube is controlled in dissimilar ways by actin filaments and microtubules. Plant Physiol. **155:** 1169–1190.

Camacho, L., and Malhó, R. (2003). Endo/exocytosis in the pollen tube apex is differentially regulated by Ca^{2+} and GTPases. J. Exp. Bot. **54:** 83–92.

Cárdenas, L., Lovy-Wheeler, A., Kunkel, J.G., and Hepler, P.K. (2008). Pollen tube growth oscillations and intracellular calcium levels are reversibly modulated by actin polymerization. Plant Physiol. **146:** 1611–1621.

Cárdenas, L., Lovy-Wheeler, A., Wilsen, K.L., and Hepler, P.K. (2005). Actin polymerization promotes the reversal of streaming in the apex of pollen tubes. Cell Motil. Cytoskeleton **61:** 112–127.

Chen, C.Y., Cheung, A.Y., and Wu, H.M. (2003). Actin-depolymerizing factor mediates Rac/Rop GTPase-regulated pollen tube growth. Plant Cell **15:** 237–249.

Chen, C.Y., Wong, E.I., Vidali, L., Estavillo, A., Hepler, P.K., Wu, H.M., and Cheung, A.Y. (2002). The regulation of actin organization by actin-depolymerizing factor in elongating pollen tubes. Plant Cell **14:** 2175–2190.

Chen, N., Qu, X., Wu, Y., and Huang, S. (2009). Regulation of actin dynamics in pollen tubes: Control of actin polymer level. J. Integr. Plant Biol. **51:** 740–750.

Cheung, A.Y., Chen, C.Y., Glaven, R.H., de Graaf, B.H., Vidali, L., Hepler, P.K., and Wu, H.M. (2002). Rab2 GTPase regulates vesicle trafficking between the endoplasmic reticulum and the Golgi bodies and is important to pollen tube growth. Plant Cell **14:** 945–962.

Cheung, A.Y., Duan, Q.H., Costa, S.S., de Graaf, B.H., Di Stilio, V.S., Feijo, J., and Wu, H.M. (2008). The dynamic pollen tube cytoskeleton: Live cell studies using actin-binding and microtubule-binding reporter proteins. Mol. Plant **1:** 686–702.

Cheung, A.Y., Niroomand, S., Zou, Y., and Wu, H.M. (2010). A transmembrane formin nucleates subapical actin assembly and controls tip-focused growth in pollen tubes. Proc. Natl. Acad. Sci. USA **107:** 16390–16395.

Cheung, A.Y., and Wu, H, M. (2001). Plant biology. Pollen tube guidance—right on target. Science **293:** 1441–1442.

Cheung, A.Y., and Wu, H.M. (2004). Overexpression of an *Arabidopsis* formin stimulates supernumerary actin cable formation from pollen tube cell membrane. Plant Cell **16:** 257–269.

Cheung, A.Y., and Wu, H.M. (2008). Structural and signaling networks for the polar cell growth machinery in pollen tubes. Annu. Rev. Plant Biol. **59:** 547–572.

Clough, S.J., and Bent, A.F. (1998). Floral dip: A simplified method for Agrobacterium-mediated transformation of *Arabidopsis thaliana*. Plant J. **16:** 735–743.

Coelho, P.C., and Malhó, R. (2006). Correlative analysis of [Ca](C) and apical secretion during pollen tube growth and reorientation. Plant Signal. Behav. **1:** 152–157.

Daher, F.B., and Geitmann, A. (2012). Actin depolymerizing factors ADF7 and ADF10 play distinct roles during pollen development and pollen tube growth. Plant Signal. Behav. **7:** 879–881.

Deeks, M.J., Fendrych, M., Smertenko, A., Bell, K.S., Oparka, K., Cvrcková, F., Zársky, V., and Hussey, P.J. (2010). The plant formin AtFH4 interacts with both actin and microtubules, and contains a newly identified microtubule-binding domain. J. Cell Sci. **123:** 1209–1215.

de Graaf, B.H., Cheung, A.Y., Andreyeva, T., Levasseur, K., Kieliszewski, M., and Wu, H.M. (2005). Rab11 GTPase-regulated membrane trafficking is crucial for tip-focused pollen tube growth in tobacco. Plant Cell **17:** 2564–2579.

Dhonukshe, P., et al. (2008). Auxin transport inhibitors impair vesicle motility and actin cytoskeleton dynamics in diverse eukaryotes. Proc. Natl. Acad. Sci. USA **105:** 4489–4494.

Fan, L.M., Wang, Y.F., Wang, H., and Wu, W.H. (2001). In vitro *Arabidopsis* pollen germination and characterization of the inward potassium currents in *Arabidopsis* pollen grain protoplasts. J. Exp. Bot. **52:** 1603–1614.

Franklin-Tong, V.E. (1999). Signaling and the modulation of pollen tube growth. Plant Cell **11:** 727–738.

Fu, Y. (2010). The actin cytoskeleton and signaling network during pollen tube tip growth. J. Integr. Plant Biol. **52:** 131–137.

Fu, Y., Wu, G., and Yang, Z. (2001). Rop GTPase-dependent dynamics of tip-localized F-actin controls tip growth in pollen tubes. J. Cell Biol. **152:** 1019–1032.

Geitmann, A., and Emons, A.M. (2000). The cytoskeleton in plant and fungal cell tip growth. J. Microsc. **198:** 218–245.

Gibbon, B.C., Kovar, D.R., and Staiger, C.J. (1999). Latrunculin B has different effects on pollen germination and tube growth. Plant Cell **11:** 2349–2363.

Gordon-Weeks, P.R., and Fischer, I. (2000). MAP1B expression and microtubule stability in growing and regenerating axons. Microsc. Res. Tech. **48:** 63–74.

Gossot, O., and Geitmann, A. (2007). Pollen tube growth: Coping with mechanical obstacles involves the cytoskeleton. Planta **226:** 405–416.

Gu, Y., Fu, Y., Dowd, P., Li, S., Vernoud, V., Gilroy, S., and Yang, Z. (2005). A Rho family GTPase controls actin dynamics and tip growth via two counteracting downstream pathways in pollen tubes. J. Cell Biol. **169:** 127–138.

Henty, J.L., Bledsoe, S.W., Khurana, P., Meagher, R.B., Day, B., Blanchoin, L., and Staiger, C.J. (2011). *Arabidopsis* actin depolymerizing factor4 modulates the stochastic dynamic behavior of actin filaments in the cortical array of epidermal cells. Plant Cell **23:** 3711–3726.

Hepler, P.K., Vidali, L., and Cheung, A.Y. (2001). Polarized cell growth in higher plants. Annu. Rev. Cell Dev. Biol. **17:** 159–187.

Higaki, T., Kutsuna, N., Sano, T., Kondo, N., and Hasezawa, S. (2010). Quantification and cluster analysis of actin cytoskeletal structures in plant cells: role of actin bundling in stomatal movement during diurnal cycles in *Arabidopsis* guard cells. Plant J. **61:** 156–165.

Holdaway-Clarke, T.L., Weddle, N.M., Kim, S., Robi, A., Parris, C., Kunkel, J.G., and Hepler, P.K. (2003). Effect of extracellular calcium, pH and borate on growth oscillations in Lilium formosanum pollen tubes. J. Exp. Bot. **54:** 65–72.

Huang, S., Blanchoin, L., Kovar, D.R., and Staiger, C.J. (2003). *Arabidopsis* capping protein (AtCP) is a heterodimer that regulates assembly at the barbed ends of actin filaments. J. Biol. Chem. **278:** 44832–44842.

Huang, S., Jin, L., Du, J., Li, H., Zhao, Q., Ou, G., Ao, G., and Yuan, M. (2007). SB401, a pollen-specific protein from *Solanum berthaultii*, binds to and bundles microtubules and F-actin. Plant J. **51:** 406–418.

Hulskamp, M., Schneitz, K., and Pruitt, R.E. (1995). Genetic evidence for a long-range activity that directs pollen tube guidance in *Arabidopsis*. Plant Cell **7:** 57–64.

Hussey, P.J., Ketelaar, T., and Deeks, M.J. (2006). Control of the actin cytoskeleton in plant cell growth. Annu. Rev. Plant Biol. **57:** 109–125.

Hwang, J.U., Gu, Y., Lee, Y.J., and Yang, Z. (2005). Oscillatory ROP GTPase activation leads the oscillatory polarized growth of pollen tubes. Mol. Biol. Cell **16:** 5385–5399.

Iwano, M., Entani, T., Shiba, H., Kakita, M., Nagai, T., Mizuno, H., Miyawaki, A., Shoji, T., Kubo, K., Isogai, A., and Takayama, S. (2009). Fine-tuning of the cytoplasmic Ca^{2+} concentration is essential for pollen tube growth. Plant Physiol. **150:** 1322–1334.

Justus, C.D., Anderhag, P., Goins, J.L., and Lazzaro, M.D. (2004). Microtubules and microfilaments coordinate to direct a fountain streaming pattern in elongating conifer pollen tube tips. Planta **219:** 103–109.

Kaothien, P., Ok, S.H., Shuai, B., Wengier, D., Cotter, R., Kelley, D., Kiriakopolos, S., Muschietti, J., and McCormick, S. (2005). Kinase partner protein interacts with the LePRK1 and LePRK2 receptor kinases and plays a role in polarized pollen tube growth. Plant J. **42:** 492–503.

Kato, M., Nagasaki-Takeuchi, N., Ide, Y., and Maeshima, M. (2010). An *Arabidopsis* hydrophilic $Ca^{2(+)}$ -binding protein with a PEVK-rich domain, PCaP2, is associated with the plasma membrane and interacts with calmodulin and phosphatidylinositol phosphates. Plant Cell Physiol. **51:** 366–379.

Khurana, P., Henty, J.L., Huang, S., Staiger, A.M., Blanchoin, L., and Staiger, C.J. (2010). *Arabidopsis* VILLIN1 and VILLIN3 have overlapping and distinct activities in actin bundle formation and turnover. Plant Cell **22:** 2727–2748.

Kost, B., Lemichez, E., Spielhofer, P., Hong, Y., Tolias, K., Carpenter, C., and Chua, N.H. (1999). Rac homologues and compartmentalized phosphatidylinositol 4, 5-bisphosphate act in a common pathway to regulate polar pollen tube growth. J. Cell Biol. **145:** 317–330.

Kroeger, J.H., Daher, F.B., Grant, M., and Geitmann, A. (2009). Microfilament orientation constrains vesicle flow and spatial distribution in growing pollen tubes. Biophys. J. **97:** 1822–1831.

Lee, Y.J., Szumlanski, A., Nielsen, E., and Yang, Z. (2008). Rho-GTPase-dependent filamentous actin dynamics coordinate vesicle targeting and exocytosis during tip growth. J. Cell Biol. **181:** 1155–1168.

Li, J., Henty-Ridilla, J.L., Huang, S., Wang, X., Blanchoin, L., and Staiger, C.J. (2012). Capping protein modulates the dynamic behavior of actin filaments in response to phosphatidic acid in *Arabidopsis*. Plant Cell **24:** 3742–3754.

Li, J., Wang, X., Qin, T., Zhang, Y., Liu, X., Sun, J., Zhou, Y., Zhu, L., Zhang, Z., Yuan, M., and Mao, T. (2011). MDP25, a novel calcium regulatory protein, mediates hypocotyl cell elongation by destabilizing cortical microtubules in *Arabidopsis*. Plant Cell **23:** 4411–4427.

Li, Y., Shen, Y., Cai, C., Zhong, C., Zhu, L., Yuan, M., and Ren, H. (2010). The type II *Arabidopsis* formin14 interacts with microtubules and microfilaments to regulate cell division. Plant Cell **22:** 2710–2726.

Liu, B.Q., Jin, L., Zhu, L., Li, J., Huang, S., and Yuan, M. (2009). Phosphorylation of microtubule-associated protein SB401 from *Solanum berthaultii* regulates its effect on microtubules. J. Integr. Plant Biol. **51:** 235–242.

Mack, T.G., Koester, M.P., and Pollerberg, G.E. (2000). The microtubule-associated protein MAP1B is involved in local stabilization of turning growth cones. Mol. Cell. Neurosci. **15:** 51–65.

McKenna, S.T., Kunkel, J.G., Bosch, M., Rounds, C.M., Vidali, L., Winship, L.J., and Hepler, P.K. (2009). Exocytosis precedes and predicts the increase in growth in oscillating pollen tubes. Plant Cell **21:** 3026–3040.

Monteiro, D., Liu, Q., Lisboa, S., Scherer, G.E., Quader, H., and Malhó, R. (2005). Phosphoinositides and phosphatidic acid regulate pollen tube growth and reorientation through modulation of $[Ca^{2+}]_c$ and membrane secretion. J. Exp. Bot. **56:** 1665–1674.

Petrásek, J., and Schwarzerová, K. (2009). Actin and microtubule cytoskeleton interactions. Curr. Opin. Plant Biol. **12:** 728–734.

Pierson, E.S., Miller, D.D., Callaham, D.A., Shipley, A.M., Rivers, B.A., Cresti, M., and Hepler, P.K. (1994). Pollen tube growth is coupled to the extracellular calcium ion flux and the intracellular calcium gradient: Effect of BAPTA-type buffers and hypertonic media. Plant Cell **6:** 1815–1828.

Ren, H., and Xiang, Y. (2007). The function of actin-binding proteins in pollen tube growth. Protoplasma **230:** 171–182.

Riederer, B.M. (2007). Microtubule-associated protein 1B, a growth-associated and phosphorylated scaffold protein. Brain Res. Bull. **71:** 541–558.

Riedl, J., Crevenna, A.H., Kessenbrock, K., Yu, J.H., Neukirchen, D., Bista, M., Bradke, F., Jenne, D., Holak, T.A., Werb, Z., Sixt, M., and Wedlich-Soldner, R. (2008). Lifeact: A versatile marker to visualize F-actin. Nat. Methods **5:** 605–607.

Schiøtt, M., Romanowsky, S.M., Baekgaard, L., Jakobsen, M.K., Palmgren, M.G., and Harper, J.F. (2004). A plant plasma membrane Ca2+ pump is required for normal pollen tube growth and fertilization. Proc. Natl. Acad. Sci. USA **101:** 9502–9507.

Sousa, E., Kost, B., and Malhó, R. (2008). *Arabidopsis* phosphatidylinositol-4-monophosphate 5-kinase 4 regulates pollen tube growth and polarity by modulating membrane recycling. Plant Cell **20:** 3050–3064.

Staiger, C.J. (2000). Signaling to the actin cytoskeleton in plants. Annu. Rev. Plant Physiol. Plant Mol. Biol. **51:** 257–288.

Staiger, C.J., Poulter, N.S., Henty, J.L., Franklin-Tong, V.E., and Blanchoin, L. (2010). Regulation of actin dynamics by actin-binding proteins in pollen. J. Exp. Bot. **61:** 1969–1986.

Staiger, C.J., Sheahan, M.B., Khurana, P., Wang, X., McCurdy, D.W., and Blanchoin, L. (2009). Actin filament dynamics are dominated by rapid growth and severing activity in the *Arabidopsis* cortical array. J. Cell Biol. **184:** 269–280.

Szumlanski, A.L., and Nielsen, E. (2009). The Rab GTPase RabA4d regulates pollen tube tip growth in *Arabidopsis thaliana*. Plant Cell **21:** 526–544.

Tsvetkov, A.S., Samsonov, A., Akhmanova, A., Galjart, N., and Popov, S.V. (2007). Microtubule-binding proteins CLASP1 and CLASP2 interact with actin filaments. Cell Motil. Cytoskeleton **64:** 519–530.

Vidali, L., and Hepler, P.K. (2001). Actin and pollen tube growth. Protoplasma **215:** 64–76.

Vidali, L., McKenna, S.T., and Hepler, P.K. (2001). Actin polymerization is essential for pollen tube growth. Mol. Biol. Cell **12:** 2534–2545.

Vidali, L., Rounds, C.M., Hepler, P.K., and Bezanilla, M. (2009). Lifeact-mEGFP reveals a dynamic apical F-actin network in tip growing plant cells. PLoS ONE **4:** e5744.

Wang, X., Zhu, L., Liu, B., Wang, C., Jin, L., Zhao, Q., and Yuan, M. (2007). *Arabidopsis* MICROTUBULE-ASSOCIATED PROTEIN18 functions in directional cell growth by destabilizing cortical microtubules. Plant Cell **19:** 877–889.

Wang, Y., Zhang, W.Z., Song, L.F., Zou, J.J., Su, Z., and Wu, W.H. (2008). Transcriptome analyses show changes in gene expression to accompany pollen germination and tube growth in *Arabidopsis*. Plant Physiol. **148:** 1201–1211.

Wu, Y., Yan, J., Zhang, R., Qu, X., Ren, S., Chen, N., and Huang, S. (2010). *Arabidopsis* FIMBRIN5, an actin bundling factor, is required for pollen germination and pollen tube growth. Plant Cell **22:** 3745–3763.

Xiang, Y., Huang, X., Wang, T., Zhang, Y., Liu, Q., Hussey, P.J., and Ren, H. (2007). ACTIN BINDING PROTEIN 29 from *Lilium* pollen plays an important role in dynamic actin remodeling. Plant Cell **19:** 1930–1946.

Yokota, E., Muto, S., and Shimmen, T. (2000). Calcium-calmodulin suppresses the filamentous actin-binding activity of a 135-kilodalton actin-bundling protein isolated from lily pollen tubes. Plant Physiol. **123:** 645–654.

Yokota, E., and Shimmen, Ki.T.T. (1998). Actin-bundling protein isolated from pollen tubes of lily. Biochemical and immunocytochemical characterization. Plant Physiol. **116:** 1421–1429.

Yokota, E., Tominaga, M., Mabuchi, I., Tsuji, Y., Staiger, C.J., Oiwa, K., and Shimmen, T. (2005). Plant villin, lily P-135-ABP, possesses G-actin binding activity and accelerates the polymerization and depolymerization of actin in a Ca^{2+}-sensitive manner. Plant Cell Physiol. **46:** 1690–1703.

Yokota, E., Vidali, L., Tominaga, M., Tahara, H., Orii, H., Morizane, Y., Hepler, P.K., and Shimmen, T. (2003). Plant 115-kDa actin-filament bundling protein, P-115-ABP, is a homologue of plant villin and is widely distributed in cells. Plant Cell Physiol. **44:** 1088–1099.

Young, K.G., Thurston, S.F., Copeland, S., Smallwood, C., and Copeland, J.W. (2008). INF1 is a novel microtubule-associated formin. Mol. Biol. Cell **19:** 5168–5180.

Yu, Y., Li, Y., Li, L., Lin, J., Zheng, C., and Zhang, L. (2009). Overexpression of PwTUA1, a pollen-specific tubulin gene, increases pollen tube elongation by altering the distribution of alpha-tubulin and promoting vesicle transport. J. Exp. Bot. **60:** 2737–2749.

Zhang, H., Qu, X., Bao, C., Khurana, P., Wang, Q., Xie, Y., Zheng, Y., Chen, N., Blanchoin, L., Staiger, C.J., and Huang, S. (2010). *Arabidopsis* VILLIN5, an actin filament bundling and severing protein, is necessary for normal pollen tube growth. Plant Cell **22:** 2749–2767.

Zhang, Y., Xiao, Y., Du, F., Cao, L., Dong, H., and Ren, H. (2011). *Arabidopsis* VILLIN4 is involved in root hair growth through regulating actin organization in a Ca^{2+}-dependent manner. New Phytol. **190:** 667–682.

Zhao, Y., Yan, A., Feijó, J.A., Furutani, M., Takenawa, T., Hwang, I., Fu, Y., and Yang, Z. (2010). Phosphoinositides regulate clathrin-dependent endocytosis at the tip of pollen tubes in *Arabidopsis* and tobacco. Plant Cell **22:** 4031–4044.